

# We are IntechOpen, the world's leading publisher of Open Access books Built by scientists, for scientists

6,500

Open access books available

177,000

International authors and editors

195M

Downloads

Our authors are among the

154

Countries delivered to

TOP 1%

most cited scientists

12.2%

Contributors from top 500 universities



WEB OF SCIENCE™

Selection of our books indexed in the Book Citation Index  
in Web of Science™ Core Collection (BKCI)

Interested in publishing with us?  
Contact [book.department@intechopen.com](mailto:book.department@intechopen.com)

Numbers displayed above are based on latest data collected.  
For more information visit [www.intechopen.com](http://www.intechopen.com)



## Chapter

# Influence of Tween 80 Surfactant on the Binding of Roxatidine Acetate and Roxatidine Acetate-loaded Chitosan Nanoparticles to Lysozyme

*Mohsen T.A. Qashqoosh, Faiza A.M. Alahdal, Yahiya Kadaf Manea, Swaleha Zubair and Saeeda Naqvi*

## Abstract

The drug binding to protein is an attractive research topic. In order to assess the release of RxAc-CsNPs and their binding with lysozyme under physiological conditions, nanocomposite materials based on chitosan (Cs) and Roxatidine acetate (RxAc) in the presence Tween 80 (Tw80) surfactant were developed. The addition of Tw80 to CsNPs increased RxAc release in vitro. In this work, Stern–Volmer plot and thermodynamic results indicated that the mechanism of Lyz with RxAc and Lyz with RxAc-CsNPs was static mechanism and the main forces in both systems were hydrogen bonding and Van der Waals forces, which indicated that the binding reaction in both systems is spontaneous, exothermic and enthalpically driven. Synchronous fluorescence and CD results indicated that the RxAc and RxAc-CsNPs cause change in the secondary construction of Lyz. It was also found that the addition of Tw80 affects the binding constant of drug with protein. Finally, the molecular docking results have also been in accordance with the results of other techniques. Hence, the developed RxAc loaded Chitosan nanoparticles could be used as an effective strategy for designing and application of the antiulcer drugs. Altogether, the present study can provide an important insight for the future designing of antiulcer drugs.

**Keywords:** Roxatidine acetate, lysozyme, tween 80, chitosan nanoparticles, spectroscopy, molecular docking

## 1. Introduction

The interactions of proteins with chemicals have prompted increasing research interest in recent years. Proteins are remarkable biomolecules presenting different functions and roles. Some are specific to their biological actions whereas some are selective toward the binding site [1, 2]. Conformational changes of protein may influence its transportation, function, assembly, potential cytotoxicity, and tendency to aggregate [3, 4]. Furthermore, it has been indicated that the serum

albumin conformation will be changed upon binding with ligands or molecules, and the change shows its influence on the secondary and tertiary structures of albumins and their biological function as a carrier protein [5, 6]. Some diseases (such as Alzheimer's disease, Parkinson's disease, and amyloid disease) are related to protein misfolding [6]. The thermodynamic and kinetic study of proteins plays an important role in understanding biological functions ranging from genetic information to molecular diagnostics [7, 8]. The functions and structure of a protein are strongly related to each other and due to this, protein folding/unfolding has protruded as an important property in biochemistry and biophysics [9, 10]. Therefore, the studies of such chemicals and their bindings with proteins are of fundamental and imperative importance.

The binding of nanoscale materials with proteins has become the most common with the availability of organic polymers, inorganic nanoparticles, carbon nanotubes, etc.. Recently, the nanoparticle studies have opened new avenues to study biomolecular interactions with their applications as drug delivery, biocompatibility, diagnostics, and smart materials. The binding of nanocolloidal particles to proteins has also been formed, since the study of immunoprobes in the early 1970s [11]. Moreover, various studies of peptide or protein including lysozyme binding with nanoparticles of different sizes have been conducted. In the process, the proteins, generally, suffer a significant loss in enzyme activity and a partial loss of structure [12, 13]. Thus, it should be expected that the size of the particle plays a major role in changing protein structure and function [13]. However, no systematic study has been performed to date on the effect of Roxatidine acetate–Chitosan nanoparticles on the structure and function of Lysozyme. For this reason, we embarked on a study of protein binding with Roxatidine acetate–Chitosan nanoparticles.

Lysozyme (Lyz) (**Figure 1A**) is one of the important proteins that is found in the blood and has various functions but is similar in its tendency to bind ligands/drugs. Lyz is an antibacterial and antiviral protein found in various biological tissues and fluids, such as skin, liver, lymphatic tissues, tears, saliva, and blood of human and other animals [13, 14]. Lyz is unique in its ability to hydrolyze the  $\beta$ -1,4 glycoside bond between N-acetylglucosamine and N-acetylmuramic acid of the gram-positive bacteria, thus protecting the body against the bacterial invasion [15]. Some of its important biological roles also include antihistaminic, anti-inflammatory, and anti-neoplastic activity [15–18]. Lyz consists of 129 amino acid residues and contains six tryptophan (Trp) and three tyrosine (Tyr) residues [4, 15]. Three residues of Trp

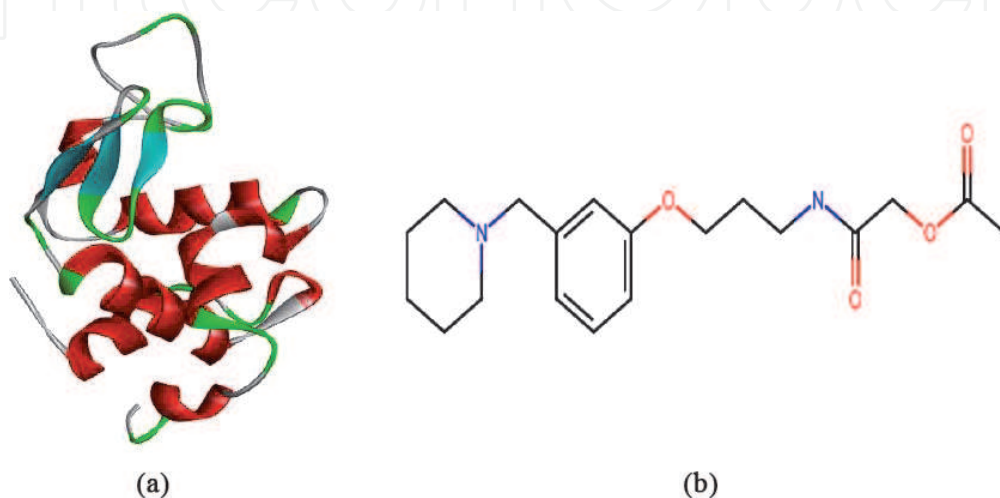


**Figure 1.**  
(A) Three dimensional structure of Lyz, (B) chemical structure of Roxatidine acetate.

are placed at the binding sites, two sites in the hydrophobic cavity, while the last site is located independently from others [4, 15, 19–21], and the effectiveness of drugs depends on both pharmacokinetic and pharmacodynamic factors. Therefore, the studies on the interactions of drugs and Lyz are of importance in understanding the release disposition, transportation, and metabolism of drug as well as the efficacy process involving drug and Lyz. Lyz has been preferentially used as a model protein to study the protein folding/unfolding, dynamics, and ligand interaction due to its small size, abundance, high stability, and ability to bind and drug carrying capacity [22–24].

Roxatidine acetate (RxAc) (**Figure 1B**) is an antagonist of a histamine H<sub>2</sub>-receptor, which rapidly turns into Roxatidine through esterases in the plasma, small intestine, and liver (its active metabolite) [25, 26]. Roxatidine is an active inhibitor of gastric acid secretion in humans and animals [3, 25] and does not overlap with other drugs in the hepatic metabolism and has no antiandrogenic influences as most other H<sub>2</sub>-receptor antagonists [27]. Wide-scale experiments have illustrated that 150 mg of Roxatidine acetate per day is recommended as typical dosages of ranitidine and cimetidine in the patients for treatment of gastric ulcer or duodenal ulcer [25, 27] and that 75 mg of Roxatidine acetate as dosage in the evening is probably a standard amount for the prohibition of peptic ulcer recurrence [25, 28]. Primary studies also mention that Roxatidine acetate is perhaps useful in the treatment of stomach ulcer and reflux esophagitis and in the protection of pulmonary acid aspiration [25].

Spectroscopic techniques are mostly used to detect the accessibility of quenchers to fluorophore groups of albumin and help to understand the binding mechanism of albumin to small molecules and clarify the nature of the binding phenomenon [11, 29].

In the present study, the RxAc and RxAcNPs interactions with Lyz were methodically investigated and analyzed using diverse spectroscopic techniques to reveal the binding types and properties of RxAc and RxAcNPs with Lyz. The influences of RxAc and RxAcNPs on the conformation and microenvironment of Lyz were explored.

The aim of this study was the synthesis and characterization of Roxatidine acetate-loaded Chitosan in the presence of Tween80 (Tw80) surfactant (RxAcNPs) and to clarify the binding mechanism of RxAc and RxAcNPs with Lyz using multi-spectroscopic and molecular docking techniques and provide useful information for understanding the toxicological actions of RxAc and RxAcNPs at the molecular level.

## 2. Experimental

### 2.1 Materials

Lysozyme (from hen egg white) (Catalog number: L6876) was purchased from Sigma and was used as such. The Lysozyme solution was prepared in the 0.1 M phosphate buffer of pH = 7.40. The concentration of Lyz was determined using the extinction coefficient  $\epsilon_{280} = 37,750 \text{ mol}^{-1} \text{ L cm}^{-1}$  [30]. Chitosan, Sodium tripolyphosphate (TPP), and Tween80 (Tw80) were also purchased from Sigma (India). NaCl (0.15 M) has been added to buffer solutions to control the ionic strength, as required. Roxatidine acetate HCl (RxAc) ( $\geq 98\%$ ) was purchased from Tokyo Chemical Industry Co., Ltd. (TCI), India. The stock solution of RxAc (0.3 mM) was prepared in ethanol and the final concentration of ethanol was below 2.3%, and the stock solution of RxAcNPs (0.3 mM) was also prepared in ethanol and

Components	Ratio (5:1:1)
Roxatidine acetate (mg)/100 ml	30
Chitosan (g)/100 ml	0.5
Sodium Tripolyphosphate (g)/100 ml	0.1
Tween 80 0.1 % (ml)	20
Acetic acid ml/100 ml	2

**Table 1.**

*Formula for preparation of Roxatidine acetate loaded Tween80-Chitosan nanoparticles.*

this concentration was used for all the spectroscopic measurements. RxAc and RxAcNPs were accurately weighed on Shimadzu AUY-220 microbalance of resolution 0.1 mg. All the reagents were of analytical grade. For all experiments, double-distilled water was used.

## 2.2 Synthesis of Roxatidine acetate nanoparticles

Roxatidine acetate drug-loaded Tween80-Chitosan nanoparticles (RxAcNPs) were prepared through the ionotropic gelation technique. The principle of this method is interaction of the positive charge of Chitosan amino groups with the negative charge of TPP groups [31, 32]. As listed in **Table 1**, the solution of Chitosan was prepared by dissolving 0.5 g Chitosan (0.5%) in 100 ml of acetic acid (1% v/v). TPP solution (0.1%) was prepared through dissolving 100 mg of TPP in 100 ml of deionized water. 30 mg of Roxatidine acetate was added to the solution of TPP. The solution was stirred at 1500 rpm for 30 min using an ultrasonicator (vibronics), and the solution of TPP was added gradually with continuous stirring for 3 hours on a homogenizer. The mixture of Roxatidine acetate, 0.1% TPP, and 0.1% Tween80 was added gradually to Chitosan solution. Tween80 was added to make the prepared solution stabilized and to limit the nanoparticle growth and thus to obtain particles of reduced mean sizes [31–33]. The precipitate was stirred at 9000 rpm for 3 hours using an ultrasonicator (vibronics). After the addition of a drug–Tween80–TPP solution to the solution of Chitosan, the suspended solution of nanoparticles was centrifuged for 15 min at 10,000 rpm, and the Roxatidine acetate nanoparticles were obtained.

## 2.3 Drug content and release profile of Roxatidine acetate nanoparticles

To confirm the drug content, encapsulation efficiency, and release of RxAc, the conventional method and dialysis method were used for testing RxAc-loaded Tween80-CsNPs. The encapsulation efficiency and drug content were estimated according to the procedure reported by Cevher et al. [34]. After drug loading, the RxAcNPs were isolated from the suspension using centrifugation at 10000 rpm for 15 min. The quantity of free Roxatidine acetate in the supernatant was measured using the UV–Vis spectrophotometer (double beam Perkin Elmer  $\lambda$ -45) at 275 nm. RxAc release was investigated in vitro by dialysis using phosphate buffer (PBS) at different pH (3.5, 6.6, 7.4, and 8.4) and 298 K. 25 mg of Roxatidine acetate-loaded Tween80–Chitosan nanoparticles were added to 50 ml of each PBS buffer in different flasks and were shaken using a magnetic stirrer at 298 K. At various time intervals, 2 ml from the suspended solution of nanoparticles was taken and centrifuged at 10000 rpm for 15 min and the standard curve for RxAc was acquired by UV spectrophotometry. At 275 nm, the RxAcNPs entrapment efficient (EE),



drug content, and accumulated release percentage (%) at different pH were determined spectrophotometrically and were calculated using the following equations, as described previously [31–35]:

$$\text{drug content (\%)} = \frac{\text{weight of drug in nanoparticles}}{\text{weight of nanoparticles}} \times 100 \quad (1)$$

$$EE (\%) = \frac{(\text{Amount of drug taken for formulation}) - (\text{amount of unentrapped drug})}{\text{Total amount of drug in formulation}} \times 100 \quad (2)$$

## 2.4 Characterization of Roxatidine acetate-loaded Tween80–Chitosan nanoparticles

Characterization of RxAc-loaded Tween80–Chitosan nanoparticles comprised Fourier transform infrared spectroscopy using PerkinElmer Frontier equipment with a resolution of  $4 \text{ cm}^{-1}$  and a wavenumber range of  $400\text{--}4000 \text{ cm}^{-1}$ . The particle size was measured by Zetasizer Nano ZS (Malvern, UK), and scanning electron microscope (SEM) in a JEOL JSM-6510 with an accelerating voltage of 15 kV was used to visualize the shape of RxAcNPs. Powder XRD scanning (Lab-X, Shimadzu-XRD 6100 instrument, Japan) was performed to analyze the crystalline nature of RxAcNPs within the range of diffraction angle  $2\theta$  from  $5^\circ$  to  $60^\circ$ .

## 2.5 Analysis of RxAc and RxAcNPs with Lyz

### 2.5.1 Fluorescence spectra study

The spectra of fluorescence emission were collected on Hitachi F-2700 Spectrofluorimeter with a Xenon lamp, and the quartz cuvette of 1 cm path length was used. The slit widths of excitation and emission were set at 5 nm. The rate of scanning was set to 300 nm/min. The wavelength of excitation was set at 280 nm and emission wavelength at 290–500 nm. The synchronous fluorescence spectra were scanned from 260 to 330 nm ( $\Delta\lambda = 15 \text{ nm}$ ) and from 220 to 330 nm ( $\Delta\lambda = 60 \text{ nm}$ ). A buffer blank spectrum was subtracted from the measured spectra for fluorescence background correction. The concentration of Lyz was kept constant at  $10 \mu\text{M}$ , while the concentrations of RxAc and RxAcNPs were varied. All the measurements were performed at pH 7.4.

### 2.5.2 The influence of Tween80 (Tw80) inclusion on the interaction of the Lyz–RxAc system

Tween80 was utilized to improve the stability of the therapeutic molecule and its safety at its target site. The influence of Tw80 inclusion on the interaction of the Lyz–RxAc system was studied by keeping the concentration of Lyz at  $10 \mu\text{M}$  and changing the concentration of RxAc ( $2\text{--}16 \mu\text{M}$ ), while the concentrations of Tw80 were maintained at 2 and  $4 \mu\text{M}$ .

### 2.5.3 UV–Vis spectroscopic measurements

The UV–Vis absorption spectra were recorded using a double-beam PerkinElmer  $\lambda\text{-45}$  spectrophotometer. For the whole experiment, the quartz cuvette of 1 cm path

length was used. The concentration of Lyz was kept at 10  $\mu\text{M}$  while the RxAc and RxAcNPs concentrations were varied. All the readings were recorded at room temperature.

#### 2.5.4 Circular dichroism (CD) measurements

Circular Dichroism (CD) spectra were carried out using a Jasco J-815 spectropolarimeter and using a quartz cell of 0.1 cm path length. Response time and data pitch were fixed at 1 s and 1 nm, respectively. CD spectra were measured in the far-UV region (200–250 nm) with a scan speed of 100 nm/min and two scans for each spectrum under constant nitrogen flow. For all the measured spectra, Phosphate buffer baseline subtraction (pH 7.4) was used. Concentration of Lyz for all runs was fixed at 10  $\mu\text{M}$ , while the RxAc and RxAcNPs concentrations were 0, 40, and 80  $\mu\text{M}$ . All the measurements were carried out at room temperature.

#### 2.5.5 Molecular docking of the Lyz–RxAc system

Molecular docking study used software Autodock 4.2 and Autodock tools (ADT) using the Lamarckian genetic algorithm [29]. The crystal structure of Lyz (PDB ID: 2LYZ) was obtained from Brookhaven Protein Data Bank and three-dimensional structure of Roxatidine acetate (CID = 5105) was obtained from PubChem. All the ions and water molecules were removed, hydrogen atoms were added, and partial Kollman charges were assigned. The Autodock run was carried out through the following parameters: GA population size, 150; maximum number of energy evolutions,  $2.5 \times 10^6$ , and Grid box size  $86 \text{ \AA} \times 80 \text{ \AA} \times 96 \text{ \AA}$  along x-, y-, and z axes covering the whole protein with a grid-point spacing of  $0.375 \text{ \AA}$ . Discovery Studio 3.5 was utilized for identification and visualization of the residues involved.

### 3. Results and discussion

#### 3.1 Method development and release profile

In order to obtain insight into the binding interaction of RxAcNPs with Lyz, the drug content, encapsulation efficiency (EE), and releasing percentage of RxAc were determined utilizing spectrophotometric techniques, with the mole ratio 5:1:1 of Cs, TPP, and Tween80, respectively. The maximum absorption wavelength was found to be 275 nm for RxAc. The drug content and encapsulation efficiency of RxAc in CsNPs based on the preparation of formulation are represented in **Table 2**. As listed in **Table 2**, the results displayed high encapsulation efficiency, which was  $88.25 \pm 0.26\%$ , and the total content of drug in the nanoform was  $26.48 \pm 0.17 \text{ mg}$ , which was nearly the total content of drug used in the preparation of the formulation matrix. These results revealed that the developed method is reliable and accurate to estimate the content of drug without interference of the formulation matrix or excipients. Additionally, it has the possibility to estimate the content of drug in the complex nanocarriers-based formulation.

The RxAc release profile from RxAc-loaded Tween80–Chitosan nanoparticles at different values of pH is illustrated in **Figure 2**. The drug released from the nanoparticles was little during the initial 2 hours (less than 25%). After 2 hours, the quantity of the released drug increased with time. The RxAc percentages released at the end of 24 hours were  $90.21 \pm 0.73$ ,  $85.83 \pm 0.54$ ,  $82.79 \pm 0.34$ , and  $75.01 \pm 0.57\%$  for pH 3.5, 6.6, 7.4, and 8.4, respectively (**Table 3** and **Figure 2**). Furthermore, as the pH decreased, the amount of released drug increased, showing

<b>The total quantity of Roxatidine acetate used in formulation (mg)</b>	<b>30.00</b>
The cumulative quantity of RxAc (mg $\pm$ SD <sup>*</sup> )	26.48 $\pm$ 0.17
Encapsulation efficiency ( % $\pm$ SD <sup>*</sup> )	88.25 $\pm$ 0.26
Particle Size (nm $\pm$ SD <sup>*</sup> )	220 $\pm$ 5

<sup>\*</sup>Standard deviation (N = 3)

**Table 2.**  
 Nanoparticle sizes and mass balance of the Roxatidine acetate used in nanoparticles formulation.

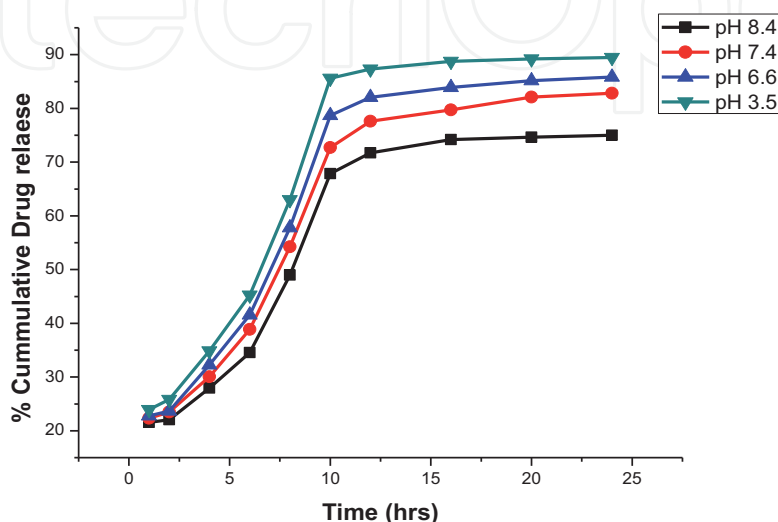


**Figure 2.**  
 In vitro of RxAcNPs release profile at different pH values.

that the drug release depends upon the pH of the media, as well as the nature of the polymer matrix [33, 34], which means that the developed method is suitable and effective for preparing the antiulcer drugs in nanoform.

The nanoparticles resulting from this developed method were used to investigate the applicability in simulation of studies of drug nanoparticles–protein interaction. The known concentrations (0–16  $\mu$ M) of the RxAcNPs solution were added to the fixed concentration of Lyz (10  $\mu$ M) to examine the binding interaction under physiological conditions.

### 3.2 Characterization of Roxatidine acetate–loaded Tween80–chitosan nanoparticles

Fourier transform infrared (FTIR) spectra of the CsNPs and RxAcNPs are shown in **Figure 3A**. Chitosan is known to possess amine groups on the glucosamine moiety whereas Roxatidine acetate is an amphoteric drug having hydrophobic and hydrophilic moieties ( $-\text{OH}$ ,  $\text{CO}$ , and  $-\text{NH}$  groups). The characteristic absorption bands for Chitosan were observed at 1650, 1545 and 1420  $\text{cm}^{-1}$  were corresponding to amide I, amide II and amide III, respectively. 1095  $\text{cm}^{-1}$  was corresponding to C–N stretching, and 2936  $\text{cm}^{-1}$  was corresponding to the asymmetric stretching vibration of methylene and 3350  $\text{cm}^{-1}$  was due to the stretching vibration of N–H. The FTIR spectra of RxAcNPs were compared with the FTIR spectra of CsNPs. The spectra did not show any new band for characteristic peaks of RxAc in RxAcNPs spectra and the existing shift of bands indicating entrapment of RxAc within the chitosan matrix, suggesting no new chemical bond formation between RxAc and CsNPs. Consequently, this observation excluded the possibility of an interaction between the polymer and drug indicating



pH Amount (mg) $\pm$ SD*	3.5	6.6	7.4	8.4
The total amount of Roxatidine acetate used for release study	25	25	25	25
The cumulative amount of drug released	20.32 $\pm$ 0.11	18.49 $\pm$ 0.39	16.82 $\pm$ 0.29	14.49 $\pm$ 0.46
Amount of drug unreleased	2.23 $\pm$ 0.24	2.97 $\pm$ 0.41	3.88 $\pm$ 0.18	4.26 $\pm$ 0.27
The total amount of drug recovered	22.55 $\pm$ 0.49	21.46 $\pm$ 0.05	20.70 $\pm$ 0.16	18.75 $\pm$ 0.21
Percentage amount of drug recovered (%)	90.21 $\pm$ 0.73	85.83 $\pm$ 0.54	82.79 $\pm$ 0.34	75.01 $\pm$ 0.57

\*Standard deviation (N = 3).

**Table 3.**  
Mass balance of Roxatidine acetate used in vitro release study at deferent pH.

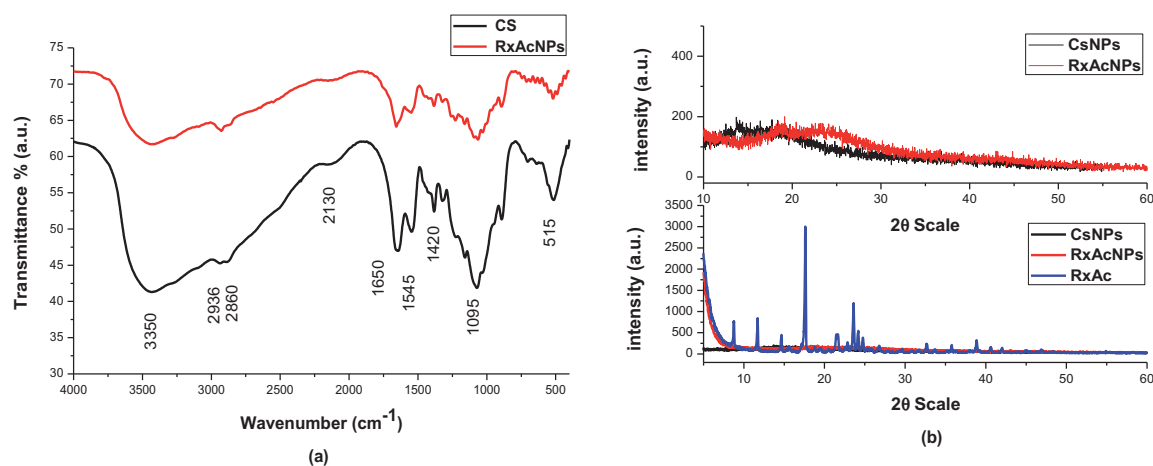


**Figure 3.**  
(a) FTIR spectra for Roxatidine acetate (RxAc), Chitosan nanoparticles (CsNPs), Roxatidine acetate loaded Chitosan nanoparticles (RxAcNPs), (b) PXRD spectra for Roxatidine acetate (RxAc), Chitosan nanoparticles (CsNPs), Roxatidine acetate loaded Chitosan nanoparticles (RxAcNPs).

that RxAc was physically dispersed in the polymer [33–38]. As shown in **Figure 3B**, RxAc-loaded Tween80–Chitosan nanoparticles were examined using the PXRD technique. The peak at  $11.72^\circ$  represents the presence of Cs and at  $17.65^\circ$ , the presence of TPP is indicated. A synthesized nanoform was specified, illustrating the semicrystalline nature of RxAcNPs after the available analysis, which depends on the little sharp pattern of XRD; hence, the drug was just encapsulated in Tween80–Cs nanoparticles without any interaction. The peaks at  $24.18^\circ$  and  $27.21^\circ$  indicated the presence of RxAc [39–45]. As shown in **Figure 4A** and **Table 2**, the data of DLS showed that the particle size of RxAcNPs was  $220 \pm 5$  nm, which was almost in conformity with the data of SEM as shown in **Figure 4B**. The SEM micrograph of RxAcNPs clearly illustrates the presence of RxAc on the Chitosan surface, which clarifies the drug encapsulation in the nanoparticle surface. The data of SEM of Tw80–CsNPs before and after loading RxAc illustrated that the spherical shape of the nanoparticles of Tw80–CsNPs is slightly deformed because of the loading of RxAc, as shown in **Figure 4B**.

### 3.3 Analysis of RxAc and RxAcNPs with Lyz

#### 3.3.1 Fluorescence spectroscopy

Fluorescence quenching of lysozyme is broadly used in measuring the binding affinity of protein and drug. Lyz has three main Trp residues located at its active

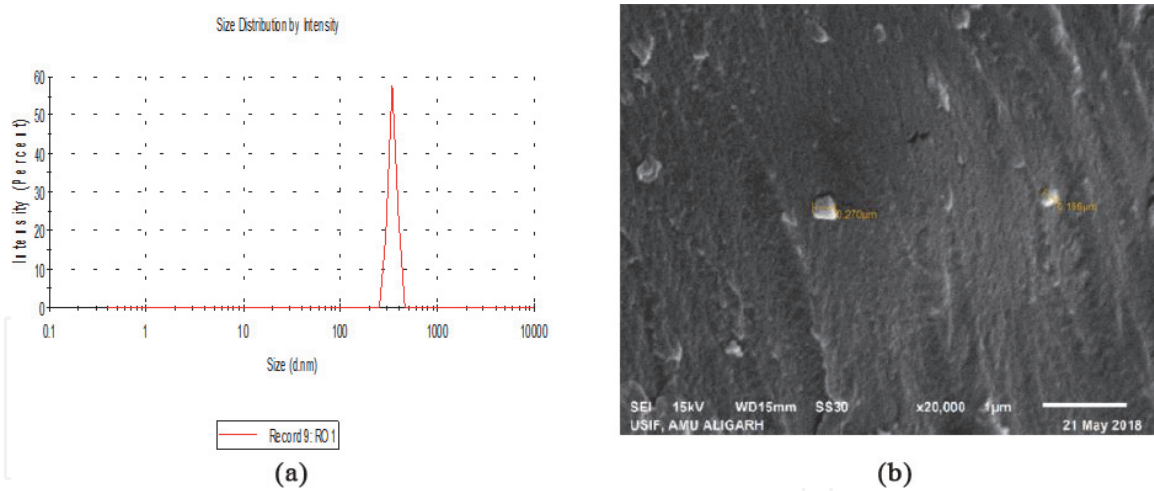


**Figure 4.** (a) Particle size distribution of RxAcNPs, (b) SEM image of RxAc-loaded Chitosan nanoparticles (RxAcNPs).

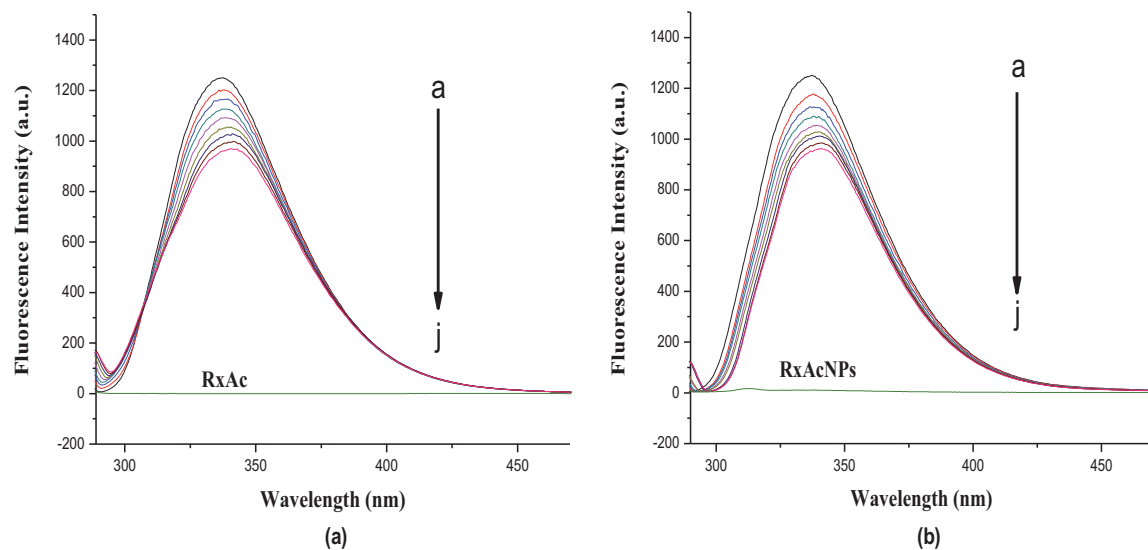


**Figure 5.** Fluorescence emission spectra of Lyz in the presence of (a) RxAc and (b) RxAcNPs at 298 K.  $C_{Lyz} : 10 \mu M$  (a),  $C_{RxAc \text{ or } RxAcNPs}$  (b-i): 2, 4, 6, 8, 10, 12, 14 and 16  $\mu M$ ; native RxAc or RxAcNPs (j): 2  $\mu M$ .

binding site, i.e., Trp-62, Trp-63, and Trp-108. The intrinsic fluorescence of Lyz comes from tryptophan residues (Trp-62, Trp-63, and Trp-108) and to study the conformational changes of Lyz in the binding process of Lyz with drugs used to be a fluorescent probe [4, 46]. The effects of RxAc and RxAcNPs on Lyz fluorescence intensity are shown in **Figure 5A** and **B**, respectively. After being excited with a wavelength of 280 nm, Lyz has a fluorescence emission with a peak at 337 nm; the fluorescent intensity of Lyz decreased regularly with increasing concentrations of RxAc and RxAcNPs. Interestingly, a red shift of about 6 nm and 4 nm in the  $\lambda_{max}$  were observed in Lyz-RxAc and Lyz-RxAcNPs systems, respectively. Moreover, 78% of the fluorescence emission was quenched by RxAc in case of the Lyz-RxAc system whereas 77% quenching of the emission was observed in case of the Lyz-RxAcNPs system, which sketches a picture as to how the quencher RxAc and RxAcNPs ingress the fluorophore and bring about the quenching. Further, it suggests a change in the surrounding environment of the fluorophores due to interaction with RxAc and RxAcNPs and that the binding regions of RxAc and RxAcNPs are in the vicinity of Trp residues. Considering the above observations, it could be

adjudged that RxAc and RxAcNPs bind to Lyz and quench its intrinsic fluorescence. The red shift in the  $\lambda_{\max}$  in Lyz–RxAc and Lyz–RxAcNPs systems indicated an increase in polarity and a decrease in hydrophobicity [47–49].

As we know well, the phenomena of fluorescence quenching are brought about by various intermolecular episodes, namely excited-state reactions, ground-state complex formation, energy-transfer molecular rearrangements, and collisional quenching [50–52]. There are two types of quenching that are Static quenching and dynamic quenching. In static quenching, a nonfluorescent fluorophore-quencher complex is formed, whereas in dynamic quenching, collision between the quencher and fluorophore during the lifetime of the excited state is established. The two types of quenching can be distinguished from each other by taking viscosity and temperature-dependent measurements [53]. In the present systems, the fluorescence-quenching mechanism has been studied using the well-known Stern–Volmer (S–V) Equation [48, 53, 54]:

$$\frac{F_0}{F} = 1 + K_{sv}[Q] = 1 + K_q\tau_0[Q] \quad (3)$$

where  $F_0$  and  $F$  are the protein fluorescence intensities in the absence and in the presence of the drug molecule (quencher), respectively,  $K_{sv}$  is the constant of Stern–Volmer quenching,  $[Q]$  is the concentration of the quencher,  $K_q$  is the quenching rate constant of the biomolecule, and  $\tau_0$  is the biomolecule average lifetime in absence of the quencher. A single type of quenching mechanism, either static or dynamic quenching mechanism, is included, when the plot of  $F_0/F$  vs.  $[Q]$  is linear, whereas deviation from linearity suggests the presence of both quenching mechanisms. The value of  $K_{sv}$  is estimated from the plot of  $F_0/F$  vs.  $[Q]$ . Considering the well-known connection between the quenching constant and the  $K_q$  quenching rate constant, and taking into account the fluorescence lifetime of the biopolymer as  $10^{-8}$  s, the  $K_q$  values can be calculated [9, 19, 55]:

$$K_q = \frac{K_{sv}}{\tau_0} \quad (4)$$

**Figure 6A** and **B** show the plots of  $F_0/F$  for Lyz versus  $[Q]$  of RxAc and RxAcNPs at 298, 304, and 310 K and pH 7.4, where  $[Q]$  ranges from 2 to 16  $\mu\text{M}$  of RxAc and RxAcNPs. Plots in **Figure 6A** and **B** show that the results of Lyz–RxAc and Lyz–RxAcNPs systems agree very well with the Stern–Volmer equation, which indicates that a single type of quenching mechanism is involved, either static or dynamic [56–59]. The results listed in **Table 4** showed that  $K_{SV}$  and  $K_q$  values of Lyz–RxAc and Lyz–RxAcNPs decreased upon increasing temperature and that the quenching of both systems follows the static quenching mechanism [53, 60]. The maximum scatter collision quenching constant ( $K_q$ ) with the biopolymer is  $2 \times 10^{10} \text{ L mol}^{-1} \text{ s}^{-1}$ . The values of  $K_q$  of the protein quenching initiated by RxAc and RxAcNPs are greater than the constant of maximum scatter collision quenching, thus indicating that quenching is initiated from the formation of complex and not the dynamic collision [53].

### 3.3.2 Binding interaction analysis

The constant of binding ( $K_a$ ) and the number of binding sites ( $n$ ) of the interaction between RxAc/RxAcNPs and Lyz could be investigated from the logarithmic form of the Stern–Volmer equation: [48, 52, 53]

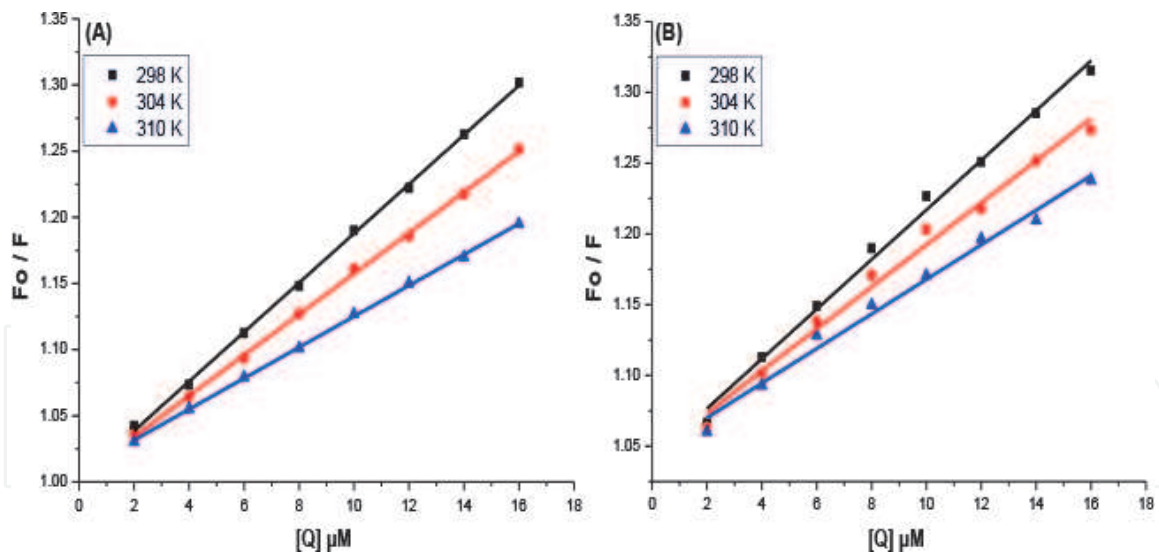


**Figure 6.** Stern-Volmer plots for quenching of Lyz fluorescence by (A) RxAc (B) RxAcNPs at different temperatures.

System	pH	T(K)	$K_{SV} \times 10^4$ (L mol <sup>-1</sup> )	$SD^*$	$R^*$	$K_q \times 10^{12}$ (L mol <sup>-1</sup> s <sup>-1</sup> )
Lyz-RxAc	7.4	298	1.86	0.04	0.999	1.86
		304	1.54	0.12	0.999	1.54
		310	1.17	0.28	0.999	1.17
Lyz-RxAcNPs	7.4	298	1.76	0.17	0.996	1.76
		304	1.49	0.13	0.994	1.49
		310	1.22	0.07	0.994	1.22
Lyz-RxAc-Tw80 (2μM)	7.4	298	1.47	0.06	0.999	1.46
Lyz-RxAc-Tw80 (4μM)	7.4	298	1.33	0.08	0.998	1.33

$S.D^*$  is standard deviation ( $N = 3$ )  
 $R^{**}$  is the correlation coefficient of  $K_{SV}$

**Table 4.** Quenching parameters of Lyz-RxAc and Lyz-RxAcNPs systems at different temperatures.

$$\log \frac{F_0 - F}{F} = \log K_a + n \log [Q] \quad (5)$$

From the plot of  $\text{Log}[(F_0 - F)/F]$  vs.  $\log [Q]$ , the binding constant ( $K_a$ ) and the number of binding sites ( $n$ ) could be obtained, where the intercept yields the value of the binding constant ( $K_a$ ) and the slope gives the number of binding sites ( $n$ ) (listed in **Table 5**). The values of  $K_a$  were  $10^4$  L mol<sup>-1</sup> for Lyz-RxAc (**Figure 7A**) indicating a high affinity of the Lyz molecule for RxAc besides binding number up to 0.96; however, the binding affinity of Lyz for RxAcNPs (**Figure 7B**) was found lower, ranging up to the order of  $10^3$  L mol<sup>-1</sup> and binding number up to 0.91. All these results lead to the conclusion that binding is stronger between Lyz and RxAc than that between Lyz and RxAcNPs, which will definitely affect its free concentration and its bound concentration in the blood plasma [61, 62].

The drug bioavailabilities could be estimated from the binding affinity values. The nanoform of drug (RxAcNPs) has shown less binding affinity to Lyz, which



System	pH	Temp. (K)	$K_a$ ( $L mol^{-1}$ )	$R^*$	$n$	$\Delta G$ ( $kJ mol^{-1}$ )	$\Delta H$ ( $kJ mol^{-1}$ )	$\Delta S$ ( $J mol^{-1} K^{-1}$ )
Lyz-RxAc	7.4	298	$1.14 \times 10^4$	0.998	0.96	-22.25	-71.80	-166.28
		304	$0.84 \times 10^4$	0.999	0.95	-21.24		
		310	$0.37 \times 10^4$	0.999	0.89	-20.25		
Lyz-RxAcNPs	7.4	298	$1.24 \times 10^3$	0.999	0.91	-17.73	-86.61	-231.13
		304	$0.69 \times 10^3$	0.999	0.88	-16.34		
		310	$0.32 \times 10^3$	0.999	0.84	-14.96		
Lyz-RxAc-Tw80 (2 $\mu M$ )	7.4	298	$2.33 \times 10^3$	0.999	0.90	-	-	-
Lyz-RxAc-Tw80 (4 $\mu M$ )	7.4	298	$1.07 \times 10^3$	0.997	0.85	-	-	-

\* $R$  is the correlation coefficient of  $K_a$

**Table 5.**

Binding constant, number of binding sites and Thermodynamic parameters of Lyz-RxAc and Lyz-RxAcNPs systems at different temperatures.

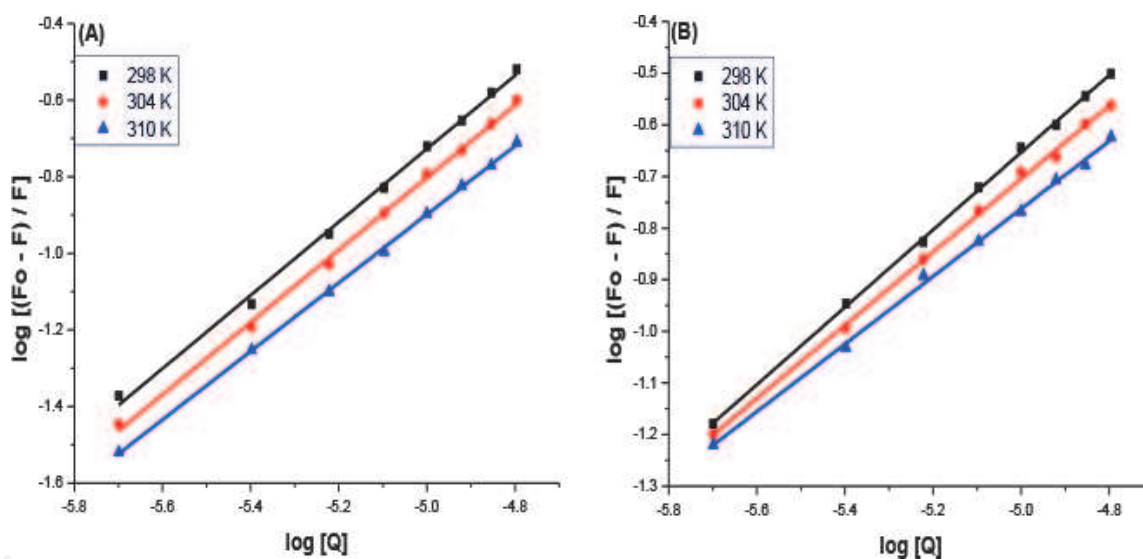


**Figure 7.**

Plots of  $\log [(F_o - F)/F]$  versus  $\log [Q]$  for (A) Lyz-RxAc and (B) Lyz-RxAcNPs systems at different temperatures.

indicates that the distribution and absorption of drug nanoparticles to various tissues will be higher, as the stability of the Lyz-RxAcNPs complex is lower compared to Lyz-RxAc complex [63, 64].

### 3.3.3 The influence of Tween80 (Tw80) inclusion on the interaction of the Lyz-RxAc system

The influence of Tween80 inclusion onto the interaction of Lyz-RxAc systems was studied by introducing Tween80 to the Lyz-RxAc system at room temperature (**Figure 8A and B**). The results of the Stern-Volmer constant ( $K_{SV}$ ) and binding constant ( $K_a$ ) are shown in **Figures 9A,B** and **10A,B** and listed in **Tables 4** and **5**. We observed that the results of  $K_{SV}$  and  $K_a$  in the presence of Tw80 were smaller than in its absence. These results indicated that the Tw80 helps to release RxAc from the Chitosan nanoparticles, due to a fraction of RxAc binding to it by weak

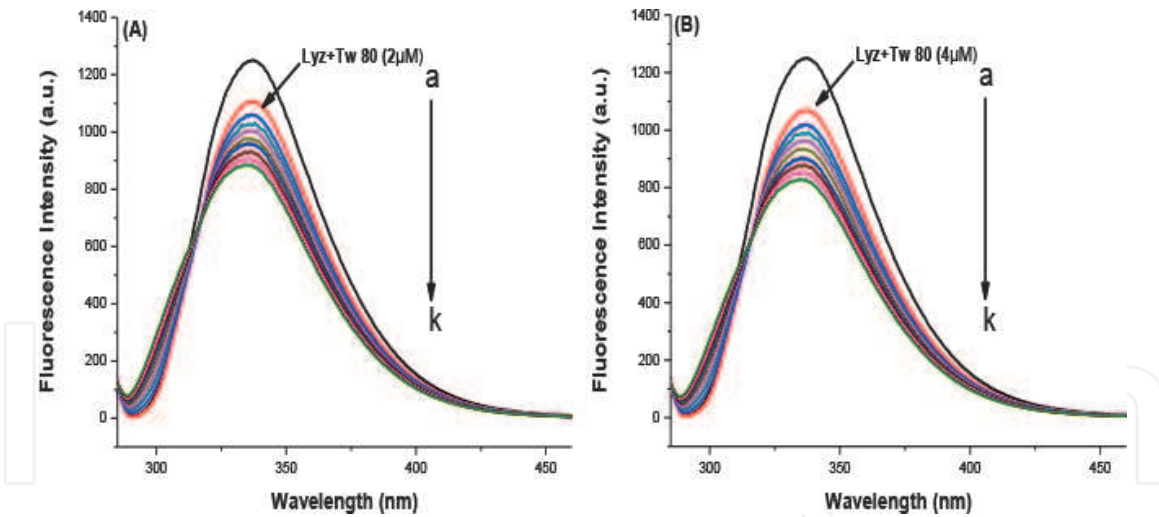


**Figure 8.**  
 A,B: Fluorescence emission spectra of Lyz in the presence of RxAc and Tw80 at 298 K. CLyz: 10 µM (a), CTw80: 2 and 4 µM (b), CRxAc (c–k): 2, 4, 6, 8, 10, 12, 14 and 16 µM.

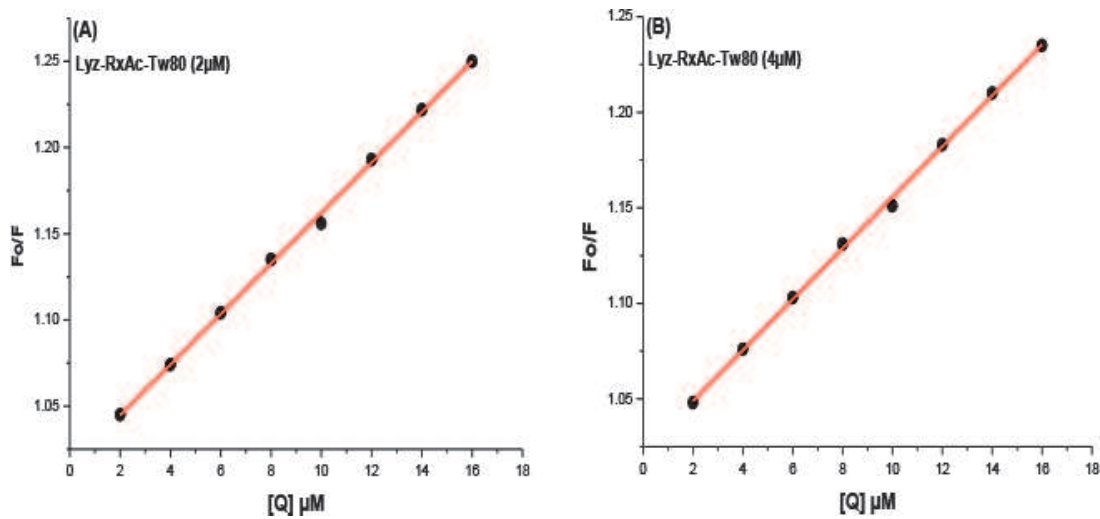


**Figure 9.**  
 A,B: Stern-Volmer plots for quenching of Lyz fluorescence by RxAc in the presence of Tw80 (2 and 4 µM) at 298 K.

bonds; hence, Tw80 helps to release more drug to the tissues as compared to the drug released from plasma [65]. Furthermore, Tw80 encloses the RxAc molecule and obstructs it from colliding directly with the amino acid residues found in the binding sites of Lyz [66].

### 3.3.4 The force acting between Lyz and RxAc/RxAcNPs

The driving force of binding could be assessed from the thermodynamic law summarized by Ross and Subramanian. The stability of the protein–drug complex and the binding of drug onto protein are influenced by various types of noncovalent forces such as hydrophobic interactions, hydrogen binding, Van der Waals, and electrostatic forces. To get the thermodynamic parameters, the Van't Hoff equation has been used:

$$\ln K_a = \frac{-\Delta H^0}{RT} + \frac{\Delta S^0}{R} \quad (6)$$

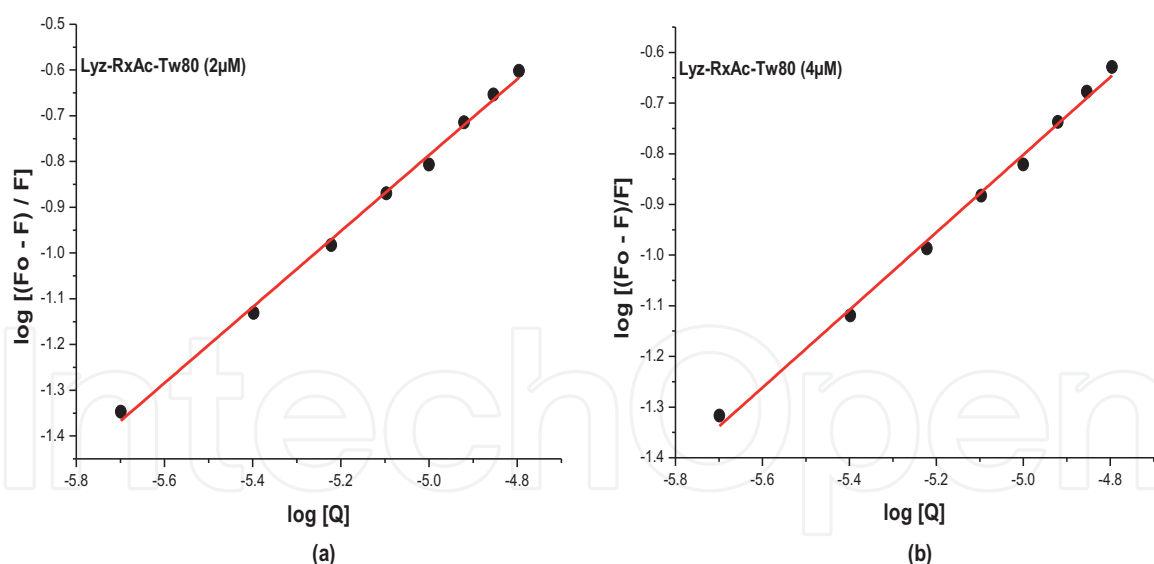


**Figure 10.**

A,B: Plots of  $\log [(F_o - F)/F]$  versus  $\log[Q]$  for Lyz-RxAc-Tw80 systems.

$$\Delta G^0 = -RT \ln K_a = \Delta H^0 - T \Delta S^0 \quad (7)$$

where  $K_a$  is the constant of binding at the corresponding temperature  $T$ ,  $T$  is the absolute temperature, and  $R$  is the universal gas constant. The plot of  $\ln K_a$  versus  $1/T$  allows the estimation of the enthalpy change ( $\Delta H$ ) and the entropy change ( $\Delta S$ ) [9, 67–69]. The enthalpy change ( $\Delta H$ ) and the entropy change ( $\Delta S$ ) can be obtained from the slope and the intercept of the Van't Hoff plots, respectively. From the thermodynamic viewpoint, Ross and Subramanian recommended that  $\Delta H < 0$  and  $\Delta S < 0$  suggest the van der Waals force and hydrogen bond formation,  $\Delta H > 0$  and  $\Delta S > 0$  show a hydrophobic interaction, and  $\Delta H < 0$  and  $\Delta S > 0$  propose electrostatic forces of interaction [53, 62–64].

As shown in **Figure 11A** and **B**, there is a good linear relationship between  $\ln K_a$  and  $1/T$ , suggesting that  $\Delta H$  is constant in the current temperature range. From **Table 5**, it could be seen that  $\Delta H = -71.80 \text{ kJ mol}^{-1}$  and  $\Delta S = -166.28 \text{ J mol}^{-1} \text{ K}^{-1}$  for the Lyz-RxAc system and  $\Delta H = -86.61 \text{ kJ mol}^{-1} \text{ K}^{-1}$  and  $\Delta S = -231.13 \text{ J mol}^{-1} \text{ K}^{-1}$  for the Lyz-RxAcNPs system. The negative values of  $\Delta H$  and  $\Delta S$  for interaction of Lyz with RxAc and Lyz with RxAcNPs indicate that hydrogen bonds and Van der Waals forces play a major role in the interaction of Lyz-RxAc and Lyz-RxAcNPs systems, and the binding reaction is exothermic and enthalpically driven. The negative values of  $\Delta G$  for both systems at different temperatures (298, 304, and 310 K) mean that the binding processes are spontaneous in both systems.

### 3.3.5 Fluorescence resonance energy transfer (FRET)

Fluorescence resonance energy transfer is a nondestructive spectroscopic method and an investigatory tool that can monitor the proximity and relative angular orientation to study energy transfer from donor to acceptor. A transfer of energy could be carried out through direct electrodynamic interaction between the primarily excited molecule and its neighbors [70, 71]. The fluorophores of donor and acceptor can be entirely nonattached or attached to the same macromolecule [72]. In the present case, Lyz is the donor and RxAc and RxAcNPs are the acceptors. According to this theory, the efficiency ( $E$ ) of energy transfer from Lyz to RxAc or RxAcNPs and the distance ( $r$ ) of binding between Lyz and RxAc or RxAcNPs could be calculated by Eq. (8) [70, 73]:

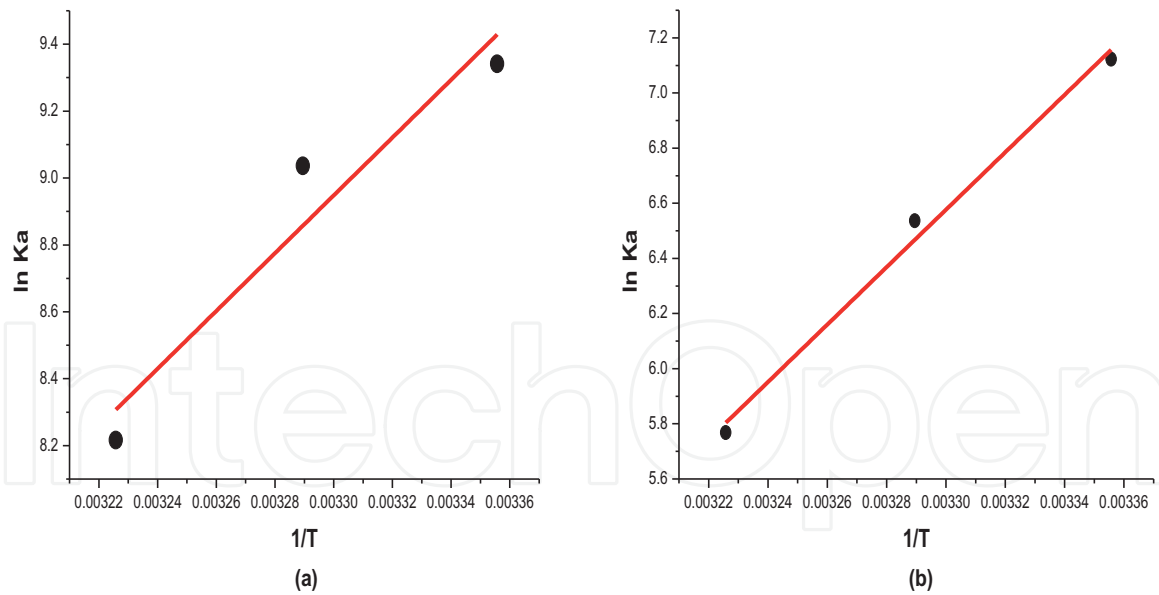


**Figure 11.** Vant-Huff Plot for (A) Lyz-RxAc and (B) Lyz-RxAcNPs systems at different temperatures.

$$E = \frac{R_0^6}{R_0^6 + r^6} = 1 - \frac{F}{F_0} \quad (8)$$

where E could be determined experimentally from the donor emission in the absence ( $F_0$ ) and presence of the acceptor (F), normalized to the same donor concentration, r is the actual distance between the donor (Lyz) and the acceptor (RxAc/RxAcNPs),  $R_0$  is the critical distance when the efficiency of transfer is 50%, which depends on the quantum yield of the donor, the extinction coefficient of the acceptor, the overlap of donor emission and acceptor absorption spectra, and the mutual orientation of the chromophores.  $R_0$  can be defined by Eq. (9) [70, 74]:

$$R_0^6 = 8.8 \times 10^{-25} K^2 N^{-4} \Phi J \quad (9)$$

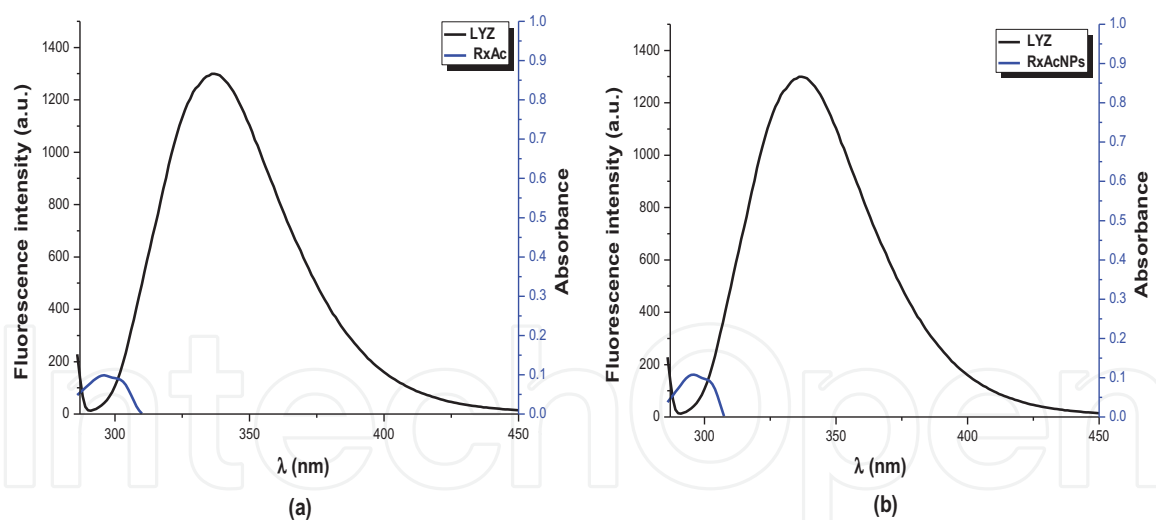
where  $K^2$  is the spatial factor of orientation related to the geometry of the donor and acceptor of dipoles, N is the refractive index of the medium,  $\Phi$  is the fluorescence quantum yield of the donor, and J is the effect of spectral overlap between the donor emission spectrum and the acceptor absorption spectrum, which could be calculated by Eq. (10)

$$J = \frac{\sum F(\lambda) \varepsilon(\lambda) \lambda^4 \Delta\lambda}{F(\lambda) \Delta\lambda} \quad (10)$$

where  $F(\lambda)$  is the donor fluorescence intensity at wavelength  $\lambda$  and  $\varepsilon(\lambda)$  is the molar absorption coefficient of the acceptor at wavelength  $\lambda$ . The efficiency of transfer (E) could be obtained using Eq.8, where F and  $F_0$  are the relative fluorescence intensities in the presence and absence of acceptor [56]. For Lyz,  $K^2 = 2/3$ ,  $N = 1.36$ , and  $\Phi = 0.15$  [62, 75].

The overlap of the absorption spectrum of RxAc and RxAcNPs with the fluorescence emission spectrum of Lyz are shown in **Figure 12A** and **B**, in the wavelength range of 280–310 nm and 280–308 nm, respectively. The fluorescence emission from both systems at an excitation wavelength of 280 nm is mainly from the Lyz molecule as both RxAc and RxAcNPs are nonfluorescent at the excitation wavelength. However, at this excitation wavelength, RxAc and RxAcNPs do show weak



**Figure 12.**

Spectral overlap between fluorescence emission spectrum of Lyz and absorption spectrum of (A) RxAc and (B) RxAcNPs when the molar ratio of Lyz and RxAc or RxAcNPs is 1:1. [Lyz]: 10  $\mu\text{M}$ , [RxAc or RxAcNPs]: 2  $\mu\text{M}$  at 298 K.

System	$R_0$ (nm)	$r$ (nm)	$E$	$J$ ( $\text{cm}^3 \text{L mol}^{-1}$ )
Lyz-RxAc	3.40	4.66	0.23	$6.67 \times 10^{-14}$
Lyz-RxAcNPs	3.44	4.53	0.24	$7.18 \times 10^{-14}$

**Table 6.**

Energy transfer parameters for Lyz-RxAc and Lyz-RxAcNPs interactions at 298 K.

absorption, which suggests the probability of energy transfer from Lyz to RxAc/RxAcNPs. Using Eqs. (8)–(10), the parameters related to energy transfer from Lyz to RxAc or RxAcNPs are calculated and are presented in **Table 6**. The values of  $R_0$ ,  $r$ ,  $J$ , and  $E$  were found to be 3.40 nm and 4.66 nm,  $6.67 \times 10^{-14} \text{ cm}^3 \text{L mol}^{-1}$  and 0.23 for Lyz–RxAc, whereas the corresponding values were 3.44 nm, 4.53 nm,  $7.18 \times 10^{-14} \text{ cm}^3 \text{L mol}^{-1}$  and 0.24 for Lyz–RxAcNPs, respectively. The obtained result indicates that RxAc and RxAcNPs are strong quenchers and these may situate in the close proximity of Lyz. The values of binding distance ( $r$ ) between the donor and acceptor for all the systems are in the range of 2–7 nm, denoting that the energy transfer is possible between Lyz and RxAc or RxAcNPs. The values of  $R_0$  and  $r$  are also in the academic range, which proves that nonradiative energy transfer occurs between Lyz and RxAc/RxAcNPs. Furthermore, the results also suggest that static quenching is responsible for the quenching of fluorescence emission as the binding involved energy transfer from Lyz to RxAc/RxAcNPs [48, 59, 76, 77].

### 3.3.6 Conformational changes of lysozyme

Synchronous fluorescence spectroscopy is a kind of important method and a proficient technique, which is utilized to evaluate the conformational changes and provides the information regarding the molecular environment in the vicinage of the chromophore molecule [78, 79]. Because of its sensitivity, spectral simplification, spectral bandwidth reduction, and shunning of different perturbing effects, it can be used as an ideal and a very useful method to study the microenvironment of Trp residues by measuring the possible shift in wavelength emission maximum ( $\lambda_{\text{em}}$ ) [48, 80]. The polarity changes around the chromophore molecule, i.e., the Lyz conformation, may be due to the shift in the position of emission maximum.

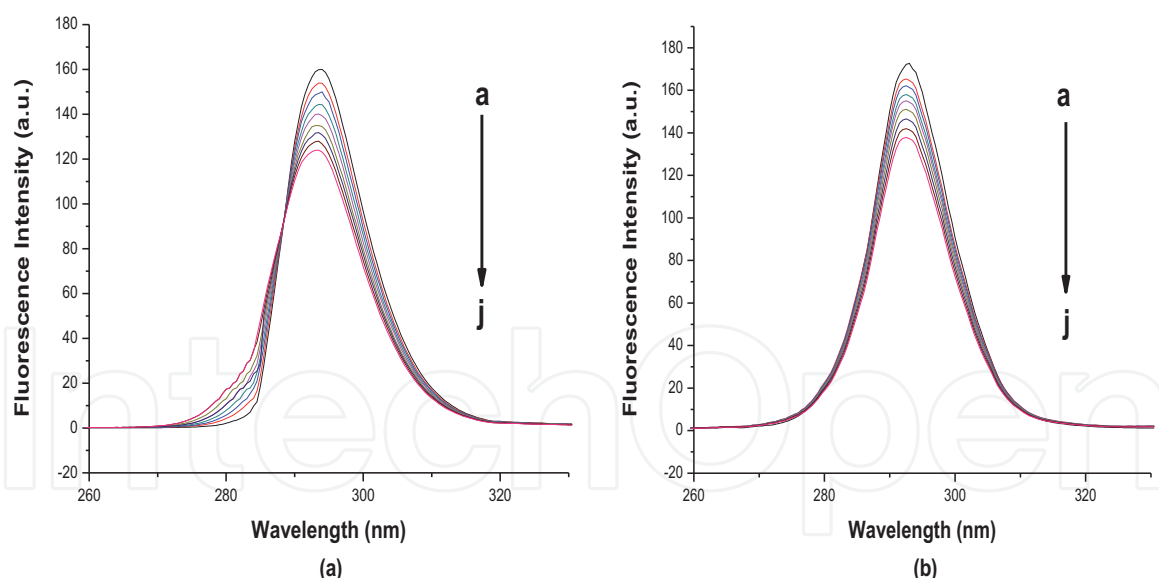


**Figure 13.** Synchronous fluorescence spectrum of (A) Lyz-RxAc and (B) Lyz-RxAcNPs systems at 298 K: ( $\Delta\lambda = 15$  nm),  $C_{(Lyz)} = 10 \mu\text{M}$ ;  $C_{(RxAc \text{ or } RxAcNPs)}$  (b-j): 2, 4, 6, 8, 10, 12, 14 and 16  $\mu\text{M}$ .

As is well-known, the spectra of synchronous fluorescence show Trp residues of Lyz at the wavelength interval ( $\Delta\lambda$ ) of 60 nm, while at the wavelength interval ( $\Delta\lambda$ ) of 15 nm, the spectra of synchronous fluorescence show Tyr residues of Lyz [81].

At  $\Delta\lambda = 15$  nm, in the Lyz-RxAc and Lyz-RxAcNPs systems in the investigated concentration range, the maximum emission wavelength keeps its position without any shift (**Figure 13A and B**), which indicates that there is no change in the microenvironment of the Tyrosine residues in both systems, whereas over the investigated concentration range at  $\Delta\lambda = 60$  nm, it can be seen that the maximum emission wavelength moderately shifts from 279 to 274 nm in the Lyz-RxAc system and from 279 to 275 nm in the Lyz-RxAcNPs system toward blue wavelengths. On looking through the synchronous spectra for the Lyz-RxAc and Lyz-RxAcNPs systems (**Figure 14A and B**), the shift effect shows that the conformation of Lyz has changed. The blue-shift effect indicates that the microenvironment around the Tryptophan residues is disturbed and shows a decrease in the polarity and an increase in the hydrophobicity around Tryptophan residues.

### 3.3.7 UV-vis absorbance spectroscopy

UV-Vis spectroscopy is a simple technique and an effective method that can help to know the structural changes in the system and to explore the formation of complex and the change in hydrophobicity [82].

In the present study, we have observed the change in the UV absorption spectra of Lyz-RxAc and Lyz-RxAcNPs systems (**Figure 15A and B**), which indicated that the interaction between Lyz and RxAc/RxAcNP molecules may lead to change in the conformation of Lyz. It was evident that the UV absorption intensity of Lyz increased regularly with the variation of RxAc and RxAcNP concentrations. The maximum peak positions of Lyz-RxAc and Lyz-RxAcNPs were shifted slightly toward a longer wavelength region (279–284 nm and 279–283 nm, respectively). The change in  $\lambda_{\text{max}}$  is observed possibly due to complex formation between Lyz and RxAc/RxAcNPs. The red shift in the absorbance spectra also indicated that the polarity of amino acid microenvironments increased with the addition of RxAc or RxAcNPs [83–86], which is in good agreement with the quenching and Synchronous fluorescence spectroscopy and thermodynamic analysis results.

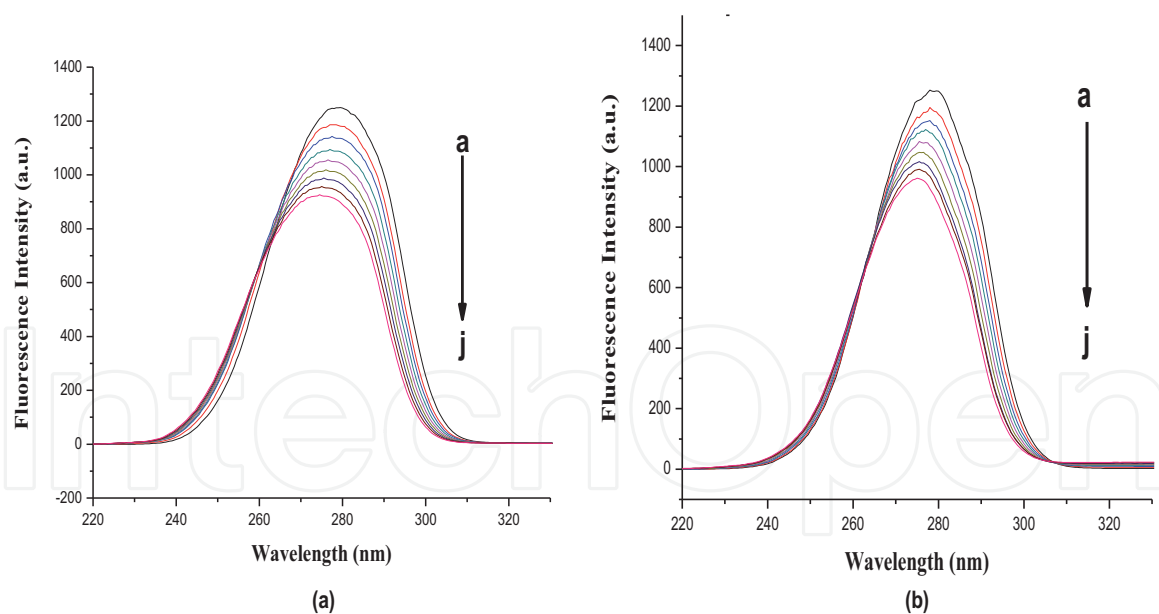


**Figure 14.** Synchronous fluorescence spectrum of (A) Lyz-RxAc and (B) Lyz-RxAcNPs systems at 298 K: ( $\Delta\lambda = 60$  nm),  $C_{\text{Lyz}} = 10 \mu\text{M}$ ;  $C_{\text{RxAc or RxAcNPs}}$  (b-j): 2, 4, 6, 8, 10, 12, 14 and 16  $\mu\text{M}$ .

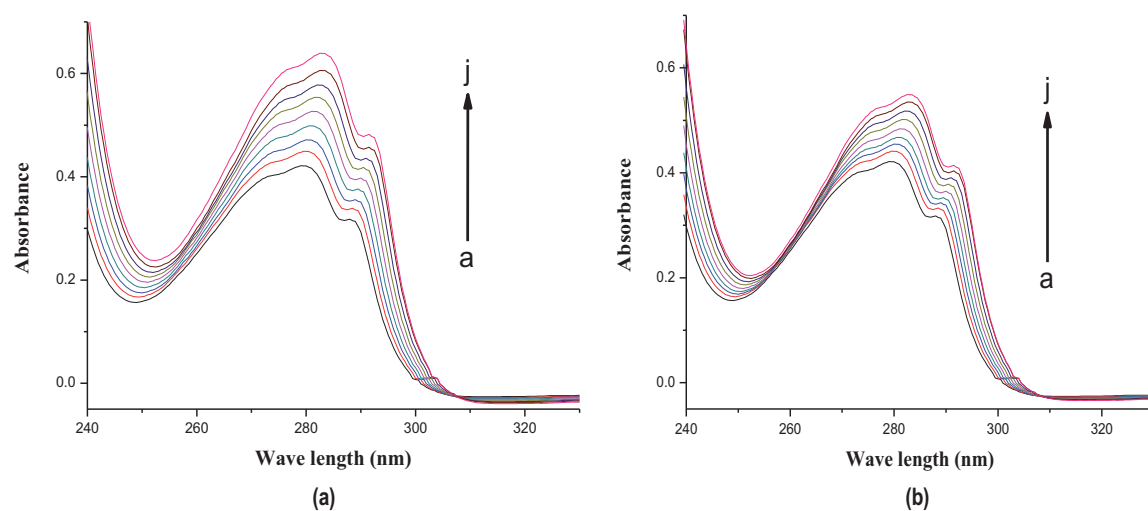


**Figure 15.** UV-Vis spectra of Lyz in the presence of (A) RxAc and (B) RxAcNPs at 298 K.  $C_{\text{Lyz}}: 10 \mu\text{M}$  (a),  $C_{\text{RxAc or RxAcNPs}}$  (b-j): 2, 4, 6, 8, 10, 12, 14 and 16  $\mu\text{M}$ .

### 3.3.8 Circular dichroism spectroscopy

The technique of far-UV Circular dichroism spectroscopy (CD) is an important and powerful technology technique utilized to probe the secondary and tertiary structures of the protein/biopolymer [87–89]. The method is used to explore the biopolymer conformational changes upon binding of RxAc and RxAcNPs to Lyz, due to its simplicity and reliability. The CD spectra of Lyz with various concentrations of RxAc and RxAcNPs have been shown in **Figure 16A** and **B** at room temperature. The results of CD spectra of Lyz show two negative bands at 208 nm ( $\pi \rightarrow \pi^*$  transition) and 229 nm ( $n \rightarrow \pi^*$  transition), which are attributed to the  $\alpha$ -helical structure of protein [67] whose magnitude reveals the amount of  $\alpha$ -helicity in Lysozyme and they arise due to  $\pi\text{-}\pi^*$  and  $n\text{-}\pi^*$  transitions of the peptide bond of  $\alpha$ -helix [84, 89–91]. The CD data have been observed in terms of mean residue ellipticity (MRE) in  $\text{deg cm}^{-2} \text{dmol}^{-1}$  according to the following Equation [92–97]:

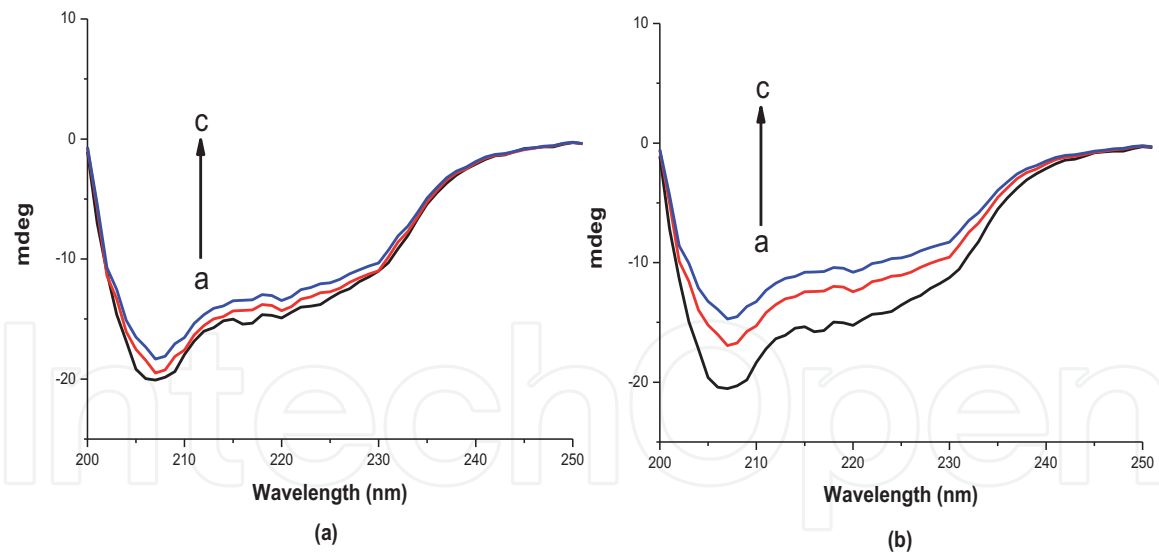


**Figure 16.** The CD spectra of (A) Lyz-RxAc and (B) Lyz-RxAcNPs systems. Lyz concentration was kept fixed at 10  $\mu\text{M}$  (a). In Lyz-RxAc and Lyz-RxAcNPs systems, RxAc or RxAcNPs concentration was fixed at 40 (b) and 80  $\mu\text{M}$  (c).

$$MRE = \frac{\text{obsCD}(m \text{ deg})}{C_p \times n \times l \times 10} \quad (11)$$

where  $C_p$  is the molar concentration of protein,  $n$  is the number of amino acid residues of the protein (129 for Lyz), and  $l$  is the path length in cm. The  $\alpha$ -helical content of Lyz is calculated from the MRE value at 208 nm, using the following Equation [92–97]:

$$\alpha - \text{helix} (\%) = \frac{-MRE_{208} - 4000}{33,000 - 4000} \times 100 \quad (12)$$

where  $MRE_{208}$  is the observed mean residue ellipticity (MRE) value at 208 nm, 4000 is the MRE of the  $\beta$ -form and random coil conformation cross at 208 nm, and 33,000 is the MRE value of a pure  $\alpha$ -helix at 208 nm.

In order to study the influence of RxAc and RxAcNPs on the secondary structure of the Lyz, the CD measurements of Lyz in the absence and presence of RxAc and RxAcNPs were performed. From **Figure 16A,B** and **Table 7**, the  $\alpha$ -helicity for free Lyz was 43.34%, while the addition of RxAc and RxAcNPs to the Lyz solution caused an increase in the negative peak ellipticities, probably as a consequence of the formation of complex between Lyz and RxAc/RxAcNPs. The CD data in the

System			$\alpha$ -helix %
[Lyz] ( $\mu\text{M}$ )	Drug	[Drug]	
		0	43.34
10	RxAc	40	41.12
		80	38.73
10	RxAcNPs	0	43.34
		40	35.82
		80	31.23

**Table 7.**  $\alpha$ -helicity (%) of Lyz at different concentrations of RxAc and RxAcNPs at 298 K.



wavelength range of 200–250 nm are used to evaluate the change of the secondary structure in Lyz. The results showed that interaction with RxAc and RxAcNPs caused only an increase in the band intensity of Lyz without any significant shift of the peaks and the helical content decreased to 38.73% and 31.23%, respectively. The decrease in the  $\alpha$ -helical content of lysozyme represents the unfolding of protein due to interaction with RxAc or RxAcNPs. The unfolding of protein changes the absorbance value, which in turn alters the ellipticity value. The results showed that Lyz was induced to adopt a more loose conformation of the extended polypeptide. The conformational transition probably resulted in the exposure of the hydrophobic cavities to more hydrophilic environment, which is favorable for the interaction between Lyz and RxAc or RxAcNPs. The CD results also corroborate the conclusion of fluorescence and UV studies [77, 98].

### 3.3.9 Molecular docking analysis

The molecular docking is an excellent and an efficient computational technique, which is used to predict the probable binding site of interaction of protein with the ligand/drug molecule and also the preferred binding site of the ligand through the 3-D graphics [4, 11, 47, 99]. Moreover, it also displays the amino acid residues encircling the ligand/drug molecule and also assists to validate the results and highlights the interaction types operating in the protein–ligand/drug system [4, 99, 100]. To study the interaction in the Lyz–RxAc system, molecular docking studies were carried out with Autodock Vina software to clarify the mode of binding between lysozyme and Roxatidine acetate and illustrate the underlying mechanism. For further study, the lowest energy was chosen that was found to be  $-5.5$  kcal/mol ( $-23.01$  kJ/mol), which is near to the experimental data of  $\Delta G^\circ$  in thermodynamic analysis ( $-22.25$  kJ/mol). In the Lyz–RxAc system (**Figure 17A and B**), the molecular docking showed the site of binding of RxAc along the long large pocket between the two domains of Lyz, which is also its site of active binding [101], and also showed that there were approximately three sites for binding of RxAc with lysozyme via hydrogen bonds at the lowest energy (Asn46 “two bonds” and Asp52 “one bond”) (**Figure 18A and B**). The three sites of binding were all located in the large pocket of lysozyme. There were two hydrogen bonds between Asn46 and RxAc that were formed; one bond was between the hydrogen atom of Asn46 and the oxygen atom (C=O) of Roxatidine acetate, and another hydrogen bond was between the other hydrogen atom of Asn46 and the oxygen atom of Roxatidine

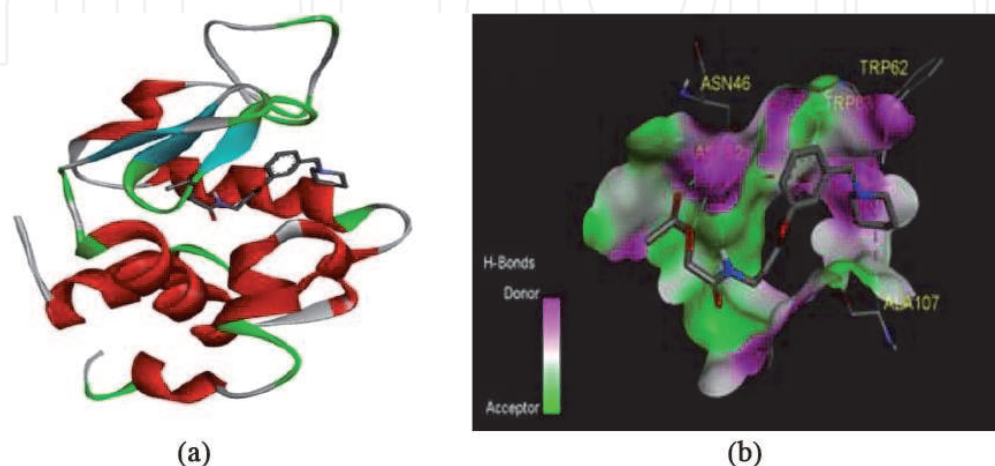


**Figure 17.** Docking interaction of Lyz-RxAc binding, (A) The lysozyme pocket when RxAc was added. (B) Gaussian contact maps superimposed with the RxAc ligand and the receptor lysozyme, hydrogen bonds preference was indicated.

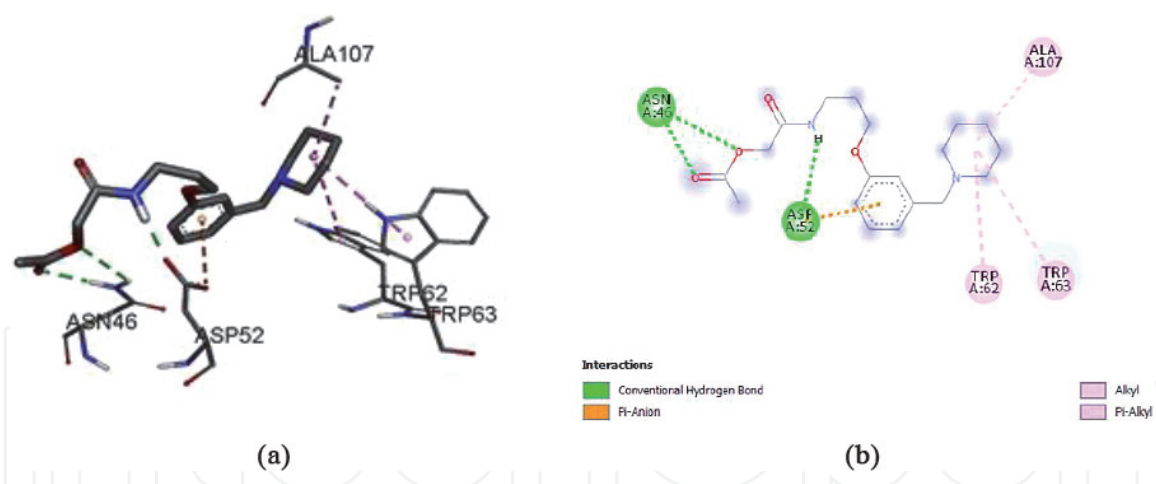


**Figure 18.** (A) Amino acid residues surrounding RxAc. (B) 2-Dimensional representation of Lyz-RxAc system.

acetate (C—O—C). The third hydrogen bond was between the oxygen atom of Asp52 and the hydrogen atom (NH) of Roxatidine acetate. The dominant fluorophores (Trp62 and Trp63) were involved in the binding sites through hydrophobic interaction via Pi-alkyl binding, which could illustrate the observed quenching of fluorescence, whereas the aliphatic amino acid (Ala107) also formed hydrophobic interaction through alkyl-alkyl binding; in addition, the oxygen atom of Asp52 formed electrostatic binding with the phenyl ring of Roxatidine acetate, as shown in **Figures 17B** and **18A,B**. Molecular docking studies have explained that hydrogen bonding was the dominant driving force in the binding of RxAc to lysozyme, and these results were in accordance with the results of thermodynamic analysis and UV spectroscopy.

#### 4. Conclusion

In the present study, the RxAc drug-loaded Tween80-Chitosan nanoparticles (RxAcNPs) have been characterized and probed through FTIR, PXRD, UV-Vis, DLS, and SEM techniques. The physicochemical properties of RxAcNPs have been employed and evaluated for drug formulation, determination of external morphology, particle size, drug content, entrapment efficiency, and in vitro release of drugs. In addition, the RxAc and RxAcNPs interactions with Lyz have been investigated utilizing spectroscopic methods such as fluorescence, UV-Vis, and CD spectroscopy. The results of Stern-Volmer plots illustrate that the interaction mechanism of Lyz-RxAc and Lyz-RxAcNPs systems was a static mechanism. In the presence of RxAc and RxAcNPs, the secondary construction of Lyz is reformed. The results of synchronous fluorescence and CD spectra confirm that the RxAc and RxAcNPs cause change in the secondary construction of Lyz. The thermodynamic results clarify that the main forces in both systems were hydrogen bonds and Van der Waals forces, also revealing that the reaction of binding in both systems is spontaneous, exothermic, and enthalpically driven. The molecular docking results were in accordance with the results of thermodynamic analysis, UV-Vis, and CD spectroscopy. The present study illustrates that the binding of RxAcNPs with Lyz is low as compared to RxAc, which confirms that the distribution and absorption of the RxAcNPs to various tissues would be higher. Therefore, the result of this study has a great importance in the clinical medicine and pharmacology area and provides important insight into the interaction of serum albumins with antiulcer drugs.

The significance of this study is evident because the developed RxAc-loaded Tween80–Chitosan nanoparticles could be utilized as an efficient strategy using nanotechnology in applications of ulcer therapy.

## **Acknowledgements**

The authors thank the Department of Chemistry and Interdisciplinary Biotechnology Unit, Aligarh Muslim University, India, for support to this work. They also thank the authorities of Aligarh Muslim University for extending the necessary facilities.

## **Conflict of interest**

The authors declare no conflict of interest.

## **Author details**

Mohsen T.A. Qashqoosh<sup>1,2\*</sup>, Faiza A.M. Alahdal<sup>1,3</sup>, Yahiya Kadaf Manea<sup>1,2</sup>, Swaleha Zubair<sup>4</sup> and Saeeda Naqvi<sup>1\*</sup>

<sup>1</sup> Department of Chemistry, Aligarh Muslim University, Aligarh, Uttar Pradesh, India


<sup>2</sup> Department of Chemistry, University of Aden, Aden, Yemen

<sup>3</sup> Department of Chemistry, Hodeidah University, Hodeidah, Yemen

<sup>4</sup> Department of Computer Science, Aligarh Muslim University, Aligarh, Uttar Pradesh, India

\*Address all correspondence to: mohssenkashkush@yahoo.com and snaqvimo2015@gmail.com

## **IntechOpen**

© 2021 The Author(s). Licensee IntechOpen. This chapter is distributed under the terms of the Creative Commons Attribution License (<http://creativecommons.org/licenses/by/3.0>), which permits unrestricted use, distribution, and reproduction in any medium, provided the original work is properly cited. 

## References

- [1] Hegyi H, Gerstein M. The relationship between protein structure and function: A comprehensive survey with application to the yeast genome. *Journal of Molecular Biology*. 1999;**288**:147-164. DOI: 10.1006/JMBI.1999.2661
- [2] Basdevant N, Weinstein H, Ceruso M. Thermodynamic basis for promiscuity and selectivity in protein-protein interactions: PDZ domains, a case study. *Journal of the American Chemical Society*. 2006;**128**:12766-12777. DOI: 10.1021/JA060830Y
- [3] He HW, Zhang J, Zhou HM, Yan YB. Conformational change in the C-terminal domain is responsible for the initiation of creatine kinase thermal aggregation. *Biophysical Journal*. 2005;**89**:2650-2658. DOI: 10.1529/biophysj.105.066142
- [4] Ansari SS, Yousuf I, Arjmand F, Siddiqi MK, Naqvi S. Exploring the intermolecular interactions and contrasting binding of flufenamic acid with hemoglobin and lysozyme: A biophysical and docking insight. *International Journal of Biological Macromolecules*. 2018;**116**:1105-1118. DOI: 10.1016/j.ijbiomac.2018.05.052
- [5] Alam P, Siddiqi K, Chaturvedi SK, Khan RH. Protein aggregation: From background to inhibition strategies. *International Journal of Biological Macromolecules*. 2017;**103**:208-219. DOI: 10.1016/j.ijbiomac.2017.05.048
- [6] Chaturvedi SK, Siddiqi MK, Alam P, Khan RH. Protein misfolding and aggregation: Mechanism, factors and detection. *Process Biochemistry*. 2016;**51**:1183-1192. DOI: 10.1016/j.procbio.2016.05.015
- [7] Sauer E, Alvarez P, Sedman J, Ramaswamy HS, Ismail AA. Heat-induced gel formation of plasma proteins: New insights by FTIR 2D correlation spectroscopy. *Food Hydrocolloids*. 2009;**23**:874-879. DOI: 10.1016/j.foodhyd.2008.03.013
- [8] Maekawa H, Toniolo C, Broxterman QB, Ge NH. Two-dimensional infrared spectral signatures of 310- And  $\alpha$ -helical peptides. *The Journal of Physical Chemistry. B*. 2007;**111**:3222-3235. DOI: 10.1021/JP0674874
- [9] Ge F, Chen C, Liu D, Han B, Xiong X, Zhao S. Study on the interaction between theasinesin and human serum albumin by fluorescence spectroscopy. *Journal of Luminescence*. 2010;**130**:168-173. DOI: 10.1016/j.jlumin.2009.08.003
- [10] Wu LZ, Ma BL, Zou DW, Tie ZX, Wang J, Wang W. Influence of metal ions on folding pathway and conformational stability of bovine serum albumin. *Journal of Molecular Structure*. 2008;**877**:44-49. DOI: 10.1016/j.molstruc.2007.07.013
- [11] Qashqoosh MTA, Alahdal FAM, Manea YK, Zakariya SM, Naqvi S. Synthesis, characterization and spectroscopic studies of surfactant loaded antiulcer drug into Chitosan nanoparticles for interaction with bovine serum albumin. *Chemical Physics*. 2019;**527**:110462. DOI: 10.1016/j.chemphys.2019.110462
- [12] Qashqoosh MTA, Manea YK, Alahdal FAM, Naqvi S. Investigation of conformational changes of Bovine Serum Albumin upon binding with Benzocaine drug: A spectral and computational analysis. *Bionanoscience*. 2019;**9**:848-858. DOI: 10.1007/S12668-019-00663-7
- [13] Vertegel AA, Siegel RW, Dordick JS. Silica nanoparticle size influences the structure and enzymatic activity of adsorbed lysozyme. *Langmuir*. 2004;**20**:6800-6807. DOI: 10.1021/LA0497200



- [14] Lee-Huang S, Maiorov V, Huang PL, Ng A, Hee CL, Chang YT, et al. Structural and functional modeling of human lysozyme reveals a unique nonapeptide, HL9, with anti-HIV activity. *Biochemistry*. 2005;**44**: 4648-4655. DOI: 10.1021/BI0477081
- [15] Das A, Thakur R, Dagar A, Chakraborty A. A spectroscopic investigation and molecular docking study on the interaction of hen egg white lysozyme with liposomes of saturated and unsaturated phosphocholines probed by an anticancer drug ellipticine. *Physical Chemistry Chemical Physics*. 2014;**16**: 5368-5381. DOI: 10.1039/c3cp54247e
- [16] Zhang HM, Chen J, Zhou QH, Shi YQ, Wang YQ. Study on the interaction between cinnamic acid and lysozyme. *Journal of Molecular Structure*. 2011;**987**:7-12. DOI: 10.1016/j.molstruc.2010.11.053
- [17] Li D, Zhang T, Xu C, Ji B. Effect of pH on the interaction of vitamin B12 with bovine serum albumin by spectroscopic approaches. *Spectrochimica Acta Part A: Molecular and Biomolecular Spectroscopy*. 2011; **83**:598-608. DOI: 10.1016/j.saa.2011.09.012
- [18] Banerjee S, Dutta Choudhury S, Dasgupta S, Basu S. Photoinduced electron transfer between hen egg white lysozyme and anticancer drug menadione. *Journal of Luminescence*. 2008;**128**:437-444. DOI: 10.1016/j.jlumin.2007.09.020
- [19] Wang W, Min W, Chen J, Wu X, Hu Z. Binding study of diprophylline with lysozyme by spectroscopic methods. *Journal of Luminescence*. 2011;**131**:820-824. DOI: 10.1016/j.jlumin.2010.12.010
- [20] Ibrahim HR, Matsuzaki T, Aoki T. Genetic evidence that antibacterial activity of lysozyme is independent of its catalytic function. *FEBS Letters*. 2001;**506**:27-32. DOI: 10.1016/S0014-5793(01)02872-1
- [21] Croguennec T, Nau F, Molle D, Le Graet Y, Brule G. Iron and citrate interactions with hen egg white lysozyme. *Food Chemistry*. 2000;**68**: 29-35. DOI: 10.1016/S0308-8146(99)00147-8
- [22] Ghosh A, Brinda KV, Vishveshwara S. Dynamics of lysozyme structure network: Probing the process of unfolding. *Biophysical Journal*. 2007; **92**:2523-2535. DOI: 10.1529/biophysj.106.099903
- [23] Zhang Z, Zheng Q, Han J, Gao G, Liu J, Gong T, et al. The targeting of 14-succinate triptolide-lysozyme conjugate to proximal renal tubular epithelial cells. *Biomaterials*. 2009;**30**: 1372-1381. DOI: 10.1016/j.biomaterials.2008.11.035
- [24] Gu Z, Zhu X, Ni S, Su Z, Zhou HM. Conformational changes of lysozyme refolding intermediates and implications for aggregation and renaturation. *The International Journal of Biochemistry & Cell Biology*. 2004; **36**:795-805. DOI: 10.1016/j.biocel.2003.08.015
- [25] Murdoch D, McTavish D. Roxatidine Acetate. *Drugs*. 1991;**42**: 240-260. DOI: 10.2165/00003495-199142020-00006
- [26] Walt RP, Logan RFA, Hawkey CJ, Daneshmend TK, Long RG, Cooper BT, et al. A comparison of roxatidine and ranitidine for the acute treatment of duodenal ulcer. *Alimentary Pharmacology & Therapeutics*. 1991;**5**: 301-307. DOI: 10.1111/J.1365-2036.1991.TB00031.X
- [27] Bickel M, Herling AW, Schoelkens B, Scholtholt J. Chemical and biologic characteristics of roxatidine acetate. *Scandinavian Journal of*



- Gastroenterology. 1988;**23**:78-88.  
DOI: 10.3109/00365528809099134
- [28] Cataldo MG, Brancato D, Donatelli M. Comparison of roxatidine and ranitidine in the treatment of refractory duodenal ulcer. *Current Therapeutic Research*. 1994;**55**:438-445. DOI: 10.1016/S0011-393X(05)80530-2
- [29] Guo X, Li X, Jiang Y, Yi L, Wu Q, Chang H, et al. A spectroscopic study on the interaction between p-nitrophenol and bovine serum albumin. *Journal of Luminescence*. 2014;**149**:353-360. DOI: 10.1016/j.jlumin.2014.01.036
- [30] Desfougères Y, Saint-Jalmes A, Salonen A, Vié V, Beaufils S, Pezennec S, et al. Strong improvement of interfacial properties can result from slight structural modifications of proteins: The case of native and dry-heated lysozyme. *Langmuir*. 2011;**27**:14947-14957. DOI: 10.1021/la203485y
- [31] Dustgania A, Farahania EV, Imanib M. Preparation of Chitosan nanoparticles loaded by Dexamethasone Sodium Phosphate. *Iranian Journal of Pharmaceutical Sciences*. 2008;**4**:111-114
- [32] Agnihotri SA, Mallikarjuna NN, Aminabhavi TM. Recent advances on chitosan-based micro- and nanoparticles in drug delivery. *Journal of Controlled Release*. 2004;**100**:5-28. DOI: 10.1016/j.jconrel.2004.08.010
- [33] Sri KV, Santhoshini G, Sankar DR, Niharika K. Formulation and evaluation of rutin loaded nanosponges. *Asian Journal of Research in Pharmaceutical Sciences*. 2018;**8**:21. DOI: 10.5958/2231-5659.2018.00005.x
- [34] Jeevitha D, Amarnath K. Chitosan/PLA nanoparticles as a novel carrier for the delivery of anthraquinone: Synthesis, characterization and in vitro cytotoxicity evaluation. *Colloids and Surfaces. B, Biointerfaces*. 2013;**101**:126-134. DOI: 10.1016/j.colsurfb.2012.06.019
- [35] Vora C, Patadia R, Mittal K, Mashru R. Formulation development, process optimization, and in vitro characterization of spray-dried lansoprazole enteric microparticles. *Scientia Pharmaceutica*. 2016;**84**:393-408. DOI: 10.3797/scipharm.1501-08
- [36] Ruckmani K, Sivakumar M, Satheesh Kumar S. Nanoparticulate drug delivery system of cytarabine hydrochloride (CTH) for improved treatment of lymphoma, in. *Journal of Biomedical Nanotechnology*. 2007;**3**(1):90-96. DOI: 10.1166/jbn.2007.016
- [37] Das S, Banerjee R, Bellare J. Aspirin loaded albumin nanoparticles by coacervation: Implications in drug delivery. *Biomaterials and Artificial Organs*. 2005;**18**(2):203-212
- [38] Nagarajan E, Shanmugasundaram P, Ravichandiran V, Vijayalakshmi A, Senthilnathan B, Masilamani K. Development and evaluation of chitosan based polymeric nanoparticles of an antiulcer drug Lansoprazole. *Journal of Applied Pharmaceutical Science*. 2015;**5**:20-25. DOI: 10.7324/JAPS.2015.50404
- [39] Elshafeey AH, Kamel AO, Awad GAS. Ammonium methacrylate units polymer content and their effect on acyclovir colloidal nanoparticles properties and bioavailability in human volunteers. *Colloids and Surfaces. B, Biointerfaces*. 2010;**75**:398-404. DOI: 10.1016/j.colsurfb.2009.08.050
- [40] Anand M, Sathyapriya P, Maruthupandy M, Hameedha Beevi A. Synthesis of chitosan nanoparticles by TPP and their potential mosquito larvicidal application. *Frontiers in Laboratory Medicine*. 2018;**2**:72-78. DOI: 10.1016/j.flm.2018.07.003

- [41] Anand M, Maruthupandy M, Kalaivani R, Suresh S, Kumaraguru AK. Larvicidal activity of Chitosan Nanoparticles Synthesized from Crab and Squilla Species against *Aedes aegypti*. *Journal of Colloid Science and Biotechnology*. 2015;**3**:188-193. DOI: 10.1166/jcsb.2014.1088
- [42] Song R, Xue R, He LH, Liu Y, Xiao QL. The structure and properties of chitosan/polyethylene glycol/silica ternary hybrid organic-inorganic films. *Chinese Journal of Polymer Science (English Edition)*. 2008;**26**:621-630. DOI: 10.1142/S0256767908003357
- [43] George M, Abraham TE. Polyionic hydrocolloids for the intestinal delivery of protein drugs: Alginate and chitosan - a review. *Journal of Controlled Release*. 2006;**114**:1-14. DOI: 10.1016/j.jconrel.2006.04.017
- [44] Namasivayam S, Robin A. Preparation of nano albumin-flutamide (Nab-flu) conjugate and evaluation of its in vitro drug control release, anticancer activity and genotoxicity. *Indian Journal of Experimental Biology*. 2018;**56**:171-179
- [45] Raj V, Prabha G. Synthesis, characterization and in vitro drug release of cisplatin loaded Cassava starch acetate-PEG/gelatin nanocomposites. *Journal of the Association of Arab Universities for Basic and Applied Sciences*. 2016;**21**: 10-16. DOI: 10.1016/j.jaubas.2015.08.001
- [46] Imoto T, Forster LS, Rupley JA, Tanaka F. Fluorescence of lysozyme: Emissions from tryptophan residues 62 and 108 and energy migration. *Proceedings of the National Academy of Sciences of the United States of America*. 1972;**69**:1151-1155. DOI: 10.1073/pnas.69.5.1151
- [47] Jing M, Song W, Liu R. Binding of copper to lysozyme: Spectroscopic, isothermal titration calorimetry and molecular docking studies. *Spectrochimica Acta Part A: Molecular and Biomolecular Spectroscopy*. 2016;**164**:103-109. DOI: 10.1016/j.saa.2016.04.008
- [48] Millan S, Satish L, Kesh S, Chaudhary YS, Sahoo H. Interaction of Lysozyme with Rhodamine B: A combined analysis of spectroscopic & molecular docking. *Journal of Photochemistry and Photobiology B: Biology*. 2016;**162**:248-257. DOI: 10.1016/j.jphotobiol.2016.06.047
- [49] Revathi R, Rameshkumar A, Sivasudha T. Spectroscopic investigations on the interactions of AgTiO<sub>2</sub> nanoparticles with lysozyme and its influence on the binding of lysozyme with drug molecule. *Spectrochimica Acta Part A: Molecular and Biomolecular Spectroscopy*. 2016;**152**:192-198. DOI: 10.1016/j.saa.2015.07.066
- [50] Siddiqi M, Nusrat S, Alam P, Malik S, Chaturvedi SK, Ajmal MR, et al. Investigating the site selective binding of busulfan to human serum albumin: Biophysical and molecular docking approaches. *International Journal of Biological Macromolecules*. 2018;**107**: 1414-1421. DOI: 10.1016/j.ijbiomac.2017.10.006
- [51] Shen H, Gu Z, Jian K, Qi J. In vitro study on the binding of gemcitabine to bovine serum albumin. *Journal of Pharmaceutical and Biomedical Analysis*. 2013;**75**:86-93. DOI: 10.1016/j.jpba.2012.11.021
- [52] Wang Z, Tan X, Chen D, Yue Q, Song Z. Study on the binding behavior of lysozyme with cephalosporin analogues by fluorescence spectroscopy. *Journal of Fluorescence*. 2009;**19**: 801-808. DOI: 10.1007/S10895-009-0477-8
- [53] Lakowicz J. Principles of fluorescence spectroscopy. 2013. DOI: 10.1007/978-0-387-46312-4

- [54] Roy S. Review on interaction of serum albumin with drug molecules research and reviews. *Journal of Pharmacology and Toxicological Studies*. 2016;**4**(2):7-16
- [55] Wang G, Hou H, Wang S, Yan C, Liu Y. Exploring the interaction of silver nanoparticles with lysozyme: Binding behaviors and kinetics. *Colloids and Surfaces. B, Biointerfaces*. 2017;**157**:138-145. DOI: 10.1016/j.colsurfb.2017.05.071
- [56] Melavanki RM, Kusanur RA, Kadadevaramath JS, Kulakarni MV. Quenching mechanisms of 5BAMC by aniline in different solvents using Stern-Volmer plots. *Journal of Luminescence*. 2009;**129**:1298-1303. DOI: 10.1016/j.jlumin.2009.06.011
- [57] Papadopoulou A, Green RJ, Frazier RA. Interaction of flavonoids with bovine serum albumin: A fluorescence quenching study. *Journal of Agricultural and Food Chemistry*. 2005;**53**:158-163. DOI: 10.1021/JF048693G
- [58] Evale BG, Hanagodimath SM. Fluorescence quenching of newly synthesized biologically active coumarin derivative by aniline in binary solvent mixtures. *Journal of Luminescence*. 2009;**129**:1174-1180. DOI: 10.1016/j.jlumin.2009.05.017
- [59] Melavanki RM, Kusanur RA, Kulakarni MV, Kadadevaramath JS. Role of solvent polarity on the fluorescence quenching of newly synthesized 7,8-benzo-4-azidomethyl coumarin by aniline in benzene-acetonitrile mixtures. *Journal of Luminescence*. 2008;**128**:573-577. DOI: 10.1016/j.jlumin.2007.08.013
- [60] Zhang Q, Ni Y, Kokot S. Competitive interactions between glucose and lactose with BSA: Which sugar is better for children? *Analyst*. 2016;**141**:2218-2227. DOI: 10.1039/c5an02420j
- [61] Sohrabi Y, Panahi-Azar V, Barzegar A, Dolatabadi JEN, Dehghan P. Spectroscopic, thermodynamic and molecular docking studies of bovine serum albumin interaction with ascorbyl palmitate food additive. *BioImpacts: BI*. 2017;**7**:241-246. DOI: 10.15171/bi.2017.28
- [62] Li D, Yang Y, Cao X, Xu C, Ji B. Investigation on the pH-dependent binding of vitamin B12 and lysozyme by fluorescence and absorbance. *Journal of Molecular Structure*. 2012;**1007**:102-112. DOI: 10.1016/j.molstruc.2011.10.028
- [63] Ercelen S, Klymchenko AS, Mély Y, Demchenko AP. The binding of novel two-color fluorescence probe FA to serum albumins of different species. *International Journal of Biological Macromolecules*. 2005;**35**:231-242. DOI: 10.1016/j.ijbiomac.2005.02.002
- [64] Naveenraj S, Anandan S. Binding of serum albumins with bioactive substances - Nanoparticles to drugs. *Journal of Photochemistry and Photobiology C Photochemistry Reviews*. 2013;**14**:53-71. DOI: 10.1016/j.jphotochemrev.2012.09.001
- [65] Zhang HX, Huang X, Zhang M. Thermodynamic studies on the interaction of dioxopromethazine to  $\beta$ -cyclodextrin and bovine serum albumin. *Journal of Fluorescence*. 2008;**18**:753-760. DOI: 10.1007/S10895-008-0348-8
- [66] Ao J, Gao L, Yuan T, Jiang G. Interaction mechanisms between organic UV filters and bovine serum albumin as determined by comprehensive spectroscopy exploration and molecular docking. *Chemosphere*. 2015;**119**:590-600. DOI: 10.1016/j.chemosphere.2014.07.019
- [67] Kumar CV, Buranaprapuk A, Sze HC, Jockusch S, Turro NJ. Chiral protein scissors: High enantiomeric selectivity for binding and its effect on



- protein photocleavage efficiency and specificity. Proceedings of the National Academy of Sciences of the United States of America. 2002;**99**:5810-5815. DOI: 10.1073/pnas.082119599
- [68] Calleri E, De Lorenzi E, Siluk D, Markuszewski M, Kaliszan R, Massolini G. Riboflavin binding protein - chiral stationary phase: Investigation of retention mechanism. Chromatographia. 2002;**55**:651-658. DOI: 10.1007/BF02491778
- [69] Fathi F, Mohammadzadeh-Aghdash H, Sohrabi Y, Dehghan P, Dolatabadi JEN. Kinetic and thermodynamic studies of bovine serum albumin interaction with ascorbyl palmitate and ascorbyl stearate food additives using surface plasmon resonance. Food Chemistry. 2018;**246**: 228-232. DOI: 10.1016/j.foodchem.2017.11.023
- [70] Chirio-Lebrun MC, Prats M. Fluorescence resonance energy transfer (FRET): Theory and experiments. Biochemical Education. 1998;**26**:320-323. DOI: 10.1016/S0307-4412(98)80010-1
- [71] Naik KM, Nandibewoor ST. Spectroscopic studies on the interaction between chalcone and bovine serum albumin. Journal of Luminescence. 2013;**143**:484-491. DOI: 10.1016/j.jlumin.2013.05.013
- [72] Howell WM, Jobs M, Brookes AJ. iFRET: An improved fluorescence system for DNA-melting analysis. Genome Research. 2002;**12**:1401-1407. DOI: 10.1101/gr.297202
- [73] Il'ichev YV, Perry JL, Simon JD. Interaction of ochratoxin a with human serum albumin. Preferential binding of the dianion and pH effects. The Journal of Physical Chemistry. B. 2002;**106**: 452-459. DOI: 10.1021/JP012314U
- [74] Zhou N, Liang YZ, Wang P. 18 $\beta$ -Glycyrrhetic acid interaction with bovine serum albumin. Journal of Photochemistry and Photobiology A: Chemistry. 2007;**185**:271-276. DOI: 10.1016/j.jphotochem.2006.06.019
- [75] Roy S. Binding behaviors of greenly synthesized silver nanoparticles – Lysozyme interaction: Spectroscopic approach. Journal of Molecular Structure. 2018;**1154**:145-151. DOI: 10.1016/j.molstruc.2017.10.048
- [76] Roy S. Binding behaviors of greenly synthesized silver nanoparticles – Lysozyme interaction: Spectroscopic approach. Journal of Molecular Structure. 2018;**1154**:145-151. DOI: 10.1016/j.molstruc.2017.10.048
- [77] Ajmal MR, Abdelhameed AS, Alam P, Khan RH. Interaction of new kinase inhibitors cabozantinib and tofacitinib with human serum alpha-1 acid glycoprotein. A comprehensive spectroscopic and molecular Docking approach. Spectrochimica Acta Part A: Molecular and Biomolecular Spectroscopy. 2016;**159**:199-208. DOI: 10.1016/j.saa.2016.01.049
- [78] Wu YL, He F, He XW, Li WY, Zhang YK. Spectroscopic studies on the interaction between CdTe nanoparticles and lysozyme, Spectrochim. Spectrochimica Acta, Part A: Molecular and Biomolecular Spectroscopy. 2008;**71**:1199-1203. DOI: 10.1016/j.saa.2008.03.018
- [79] Manea YK, Khan AMT, Qashqoosh MTA, Wani AA, Shahadat M. Ciprofloxacin-supported chitosan/polyphosphate nanocomposite to bind bovine serum albumin: Its application in drug delivery. Journal of Molecular Liquids. 2019;**292**. DOI: 10.1016/j.molliq.2019.111337
- [80] Ashoka S, Seetharamappa J, Kandagal PB, Shaikh SMT. Investigation of the interaction between trazodone hydrochloride and bovine serum albumin. Journal of Luminescence.

2006;**121**:179-186. DOI: 10.1016/j.jlumin.2005.12.001

[81] Paramaguru G, Kathiravan A, Selvaraj S, Venuvanalingam P, Renganathan R. Interaction of anthraquinone dyes with lysozyme: Evidences from spectroscopic and docking studies. *Journal of Hazardous Materials*. 2010;**175**:985-991. DOI: 10.1016/j.jhazmat.2009.10.107

[82] Bi S, Song D, Tian Y, Zhou X, Liu Z, Zhang H. Molecular spectroscopic study on the interaction of tetracyclines with serum albumins. *Spectrochimica Acta Part A: Molecular and Biomolecular Spectroscopy*. 2005;**61**:629-636. DOI: 10.1016/j.saa.2004.05.028

[83] Shaikh SMT, Seetharamappa J, Kandagal PB, Ashoka S. Binding of the bioactive component isothipendyl hydrochloride with bovine serum albumin. *Journal of Molecular Structure*. 2006;**786**:46-52. DOI: 10.1016/j.molstruc.2005.10.021

[84] Hemalatha K, Madhumitha G, Al-Dhabi NA, Arasu MV. Importance of fluorine in 2,3-dihydroquinazolinone and its interaction study with lysozyme. *Journal of Photochemistry and Photobiology B: Biology*. 2016;**162**:176-188. DOI: 10.1016/j.jphotobiol.2016.06.036

[85] Liu X, Li H. Spectroscopic studies on the interaction of polydatin with bovine serum albumin. *Asian Journal of Chemistry*. 2013;**25**:8131-8135. DOI: 10.14233/ajchem.2013.15264

[86] Jash C, Basu P, Payghan PV, Ghoshal N, Kumar GS. Chelerythrine-lysozyme interaction: Spectroscopic studies, thermodynamics and molecular modeling exploration. *Physical Chemistry Chemical Physics*. 2015;**17**:16630-16645. DOI: 10.1039/c5cp00424a

[87] Corrêa D, Ramos C. The use of circular dichroism spectroscopy to study

protein folding, form and function. *African Journal of Biochemistry Research*. 2009;**3**:164-173. DOI: 10.5897/AJBR.9000245

[88] Chaturvedi SK, Khan JM, Siddiqi MK, Alam P, Khan RH. Comparative insight into surfactants mediated amyloidogenesis of lysozyme. *International Journal of Biological Macromolecules*. 2016;**83**:315-325. DOI: 10.1016/j.ijbiomac.2015.11.053

[89] Ding F, Zhao G, Huang J, Sun Y, Zhang L. Fluorescence spectroscopic investigation of the interaction between chloramphenicol and lysozyme. *European Journal of Medicinal Chemistry*. 2009;**44**:4083-4089. DOI: 10.1016/j.ejmech.2009.04.047

[90] Rahman MH, Maruyama T, Okada T, Yamasaki K, Otagiri M. Study of interaction of carprofen and its enantiomers with human serum albumin-I. Mechanism of binding studied by dialysis and spectroscopic methods. *Biochemical Pharmacology*. 1993;**46**:1721-1731. DOI: 10.1016/0006-2952(93)90576-I

[91] Azimi O, Emami Z, Salari H, Chamani J. Probing the interaction of human serum albumin with norfloxacin in the presence of high-frequency electromagnetic fields: Fluorescence spectroscopy and circular dichroism investigations. *Molecules*. 2011;**16**:9792-9818. DOI: 10.3390/molecules16129792

[92] Greenfield NJ. Using circular dichroism spectra to estimate protein secondary structure. *Nature Protocols*. 2007;**1**:2876-2890. DOI: 10.1038/nprot.2006.202

[93] Kelly S, Price N. The use of circular dichroism in the investigation of protein structure and function. *Current Protein & Peptide Science*. 2005;**1**:349-384. DOI: 10.2174/1389203003381315



[94] Ranjbar B, Gill P. Circular dichroism techniques: Biomolecular and nanostructural analyses- A review. *Chemical Biology & Drug Design*. 2009; **74**:101-120. DOI: 10.1111/j.1747-0285.2009.00847.x

[95] Price NC. Conformational issues in the characterization of proteins. *Biotechnology and Applied Biochemistry*. 2000; **31**:29. DOI: 10.1042/BA19990102

[96] Dolatabadi JEN, Panahi-Azar V, Barzegar A, Jamali AA, Kheiridoosh F, Kashanian S, et al. Spectroscopic and molecular modeling studies of human serum albumin interaction with propyl gallate. *RSC Advances*. 2014; **4**: 64559-64564. DOI: 10.1039/c4ra11103f

[97] Bhogale A, Patel N, Mariam J, Dongre PM, Miotello A, Kothari DC. Comprehensive studies on the interaction of copper nanoparticles with bovine serum albumin using various spectroscopies. *Colloids and Surfaces. B, Biointerfaces*. 2014; **113**:276-284. DOI: 10.1016/j.colsurfb.2013.09.021

[98] Parker W, Song PS. Protein structures in SDS micelle-protein complexes. *Biophysical Journal*. 1992; **61**: 1435-1439. DOI: 10.1016/S0006-3495(92)81949-5

[99] Hernández-Santoyo A, Tenorio-Barajas AY, Altuzar V, Vivanco-Cid H, Mendoza-Barrera C. Protein engineering-technology and application. *IntechOpen*. 2013:63-81. DOI: 10.5772/56376

[100] Leelananda SP, Lindert S. Computational methods in drug discovery. *Beilstein Journal of Organic Chemistry*. 2016; **12**:2694-2718. DOI: 10.3762/bjoc.12.267

[101] Callewaert L, Michiels CW. Lysozymes in the animal kingdom. *Journal of Biosciences*. 2010; **35**:127-160. DOI: 10.1007/s12038-010-0015-5